INL/EXT-18-45222
Revision 0

Grain Size and Phase Purity Characterization of U_3Si_2 Pellet Fuel

Rita E. Hoggan, Kevin R. Tolman, Fabiola Cappia, Adrian R. Wagner,
and Jason M. Harp

May 2018

The INL is a U.S. Department of Energy National Laboratory
operated by Battelle Energy Alliance

INL/EXT-18-45222
Revision 0

Grain Size and Phase Purity Characterization of U_3Si_2 Pellet Fuel

Rita E. Hoggan, Kevin R. Tolman, Fabiola Cappia, Adrian R. Wagner, and Jason M. Harp

May 2018

Idaho National Laboratory
Idaho Falls, Idaho 83415

http://www.inl.gov

Prepared for the
U.S. Department of Energy
Office of Nuclear Energy
Under DOE Idaho Operations Office
Contract DE-AC07-05ID14517

Grain Size and Phase Purity Characterization of U_3Si_2 Pellet Fuel

INL/EXT-18-45222
Revision 0

May 2018

Approved by:

Name Title [optional]	Date
Name Title [optional]	Date
Name Title [optional]	Date
Name Title [optional]	Date

ABSTRACT

Characterization of U_3Si_2 fresh fuel pellets is important for quality assurance and validation of the finished product. Grain size measurement methods, phase identification methods using scanning electron microscopes equipped with energy dispersive spectroscopy and x-ray diffraction, and phase quantification methods via image analysis have been developed and implemented on U_3Si_2 pellet samples. A wide variety of samples have been characterized including representative pellets from an initial irradiation experiment, and samples produced using optimized methods to enhance phase purity from an extended fabrication effort. The average grain size for initial pellets was between 16 and 18 μm. The typical average grain size for pellets from the extended fabrication was between 20 and 30 μm with some samples exhibiting irregular grain growth. Pellets from the latter half of extended fabrication had a bimodal grain size distribution consisting of coarsened grains (>80 μm) surrounded by the typical (20-30 μm) grain structure around the surface. Phases identified in initial uranium silicide pellets included: U_3Si_2 as the main phase composing about 80 vol. %, Si rich phases (USi and U_5Si_4) composing about 13 vol. %, and UO_2 composing about 5 vol. %. Initial batches from the extended U_3Si_2 pellet fabrication had similar phases and phase quantities. The latter half of the extended fabrication pellet batches did not contain Si rich phases, and had between 1-5% UO_2: achieving U_3Si_2 phase purity between 95 vol. % and 98 vol. % U_3Si_2. The amount of UO_2 in sintered U_3Si_2 pellets is correlated to the length of time between U_3Si_2 powder fabrication and pellet formation. These measurements provide information necessary to optimize fabrication efforts and a baseline for future work on this fuel compound.

CONTENTS

ABSTRACT v

ACRONYMS xi

1. INTRODUCTION 1

2. MATERIALS AND METHODS 2
   - 2.1 Sample Preparation 2
     - 2.1.1 Sectioning 2
     - 2.1.2 Mounting 3
     - 2.1.3 Polishing 3
   - 2.2 Grain Size Analysis 5
     - 2.2.1 Collecting LOM Images 6
     - 2.2.2 Intercept Method 6
   - 2.3 Phase Purity and Porosity Analysis 8
     - 2.3.1 Collecting SEM Images 8
     - 2.3.2 Identifying Phases 10
     - 2.3.3 Image Analysis 12
     - 2.3.4 Automatic Image Analysis 15

3. RESULTS 17
   - 3.1 Grain Size 17
   - 3.2 Phase Purity 21

4. DISCUSSION 26

5. CONCLUSIONS 28

6. ACKNOWLEDGEMENTS 29

7. REFERENCES 29

Appendix A — Grain Size Measurement Data Record 33

Appendix B — Phase Quantification Data Record 37

FIGURES

Figure 1. Longitudinal cross section representation. 3

Figure 2. Polishing steps for a mounted U_3Si_2 pellet section. 5

Figure 3. An example of a polarized optical micrograph (1005200xlon.tif) with the circular intercept grain size determination method illustrated. 7

Figure 4. Example of micrographs from both the JEOL 7600 (top row) and the Phenom XL (bottom row) at differing magnifications to measure phases with higher magnification (left side) and pores with larger area (right side). 9

Figure 5. Examples of preparation induced pullout and as-fabricated pores. 10

Figure 6. Examples of miniscule phase impurities containing Fe, Cu, and W in a U_3Si_2 pellet sample. 11

Figure 7. Silicon elemental EDS map of an ATF-1 DU sample and corresponding SEM BSE micrograph. 12

Figure 8. BSE, SEI, and corresponding duplicated BSE images adjusted to segregate individual phases 13

Figure 9. Phase quantification image analysis process flow chart. 14

Figure 10. Grey level/phase segregation via manual and automatic image analysis shown in black and white images and the colored image (White = U_3Si_2, Red = Si rich phase, Blue = UO_2, Black = pores, Green = Fe phase) respectively. 15

Figure 11. Graphic representation of U_3Si_2 SEM image automatic analysis. 16

Figure 12. BSE and TOPO micrographs with corresponding grey level/phase segregation via automatic image analysis. (White = U_3Si_2, Blue = UO_2, Black = pores, Green = Fe phase). 17

Figure 13. Representative grains of DU and LEU pellets fabricated for ATF-1. 17

Figure 14. Grain size measurement summary for representative pellets from ATF-1 and batch samples from extended fabrication pellets. 18

Figure 15. Representative examples of U_3Si_2 grain size. 19

Figure 16. Longitudinal cross section of Sample 1437: example of bimodal grain growth with a coarse inner structure and fine outer structure. 19

Figure 17. Longitudinal cross section of Sample 1496: example of bimodal grain growth with a coarse inner structure and fine non-continuous/uniform outer structure. 20

Figure 18. Sample 1459 optical images showing irregular mixed grain growth with fine grains around the edge, very large grains just within that and large grains in the center. 20

Figure 19. Radial cross section of Sample 1476 with enlarged regions to illustrate the slight gradient in grain size distribution from edge to center. 21

Figure 20. Representation of phase measurements as a function of volume percent in U_3Si_2 pellets. 22

Figure 21. XRD spectra and BSE image of ATF-1 DU sample. 23

Figure 22. XRD spectra forSsample 1301 illustrating the main phase of U_3Si_2, the “like- U_3Si_2” phase, the U_5Si_4 phase, and the UO_2 phase. 24

Figure 23. XRD spectra illustrating the main U_3Si_2 phase, the “like- U_3Si_2” phase, the UO_2 phase, and the U_5Si_4 phase. 25

Figure 24. Extended fabrication U_3Si_2 pellet BSE micrograph examples. 25

Figure 25. SEM BSE micrograph and XRD spectra for Sample 1459 with the blue line representing the calculated U_3Si_2 spectra and the black line representing the collected spectra, and an inset showing the location of the UO_2 peaks in the collected spectra. 26

Figure 26. Correlation of volume percent UO_2 in U_3Si_2 pellets with age of U_3Si_2 powder. 26

Figure 27. Carbon content of samples from extend fabrication sorted by carbon content: low to high. 28

TABLES

Table 1. General guideline for polishing epoxy mounted U_3Si_2. 4
Table 2. Parameters used in collecting micrographs. 8
Table 3. Grain size values for samples from ATF-1 and extended fabrication pellet samples. 18
Table 4. Summary of phase measurements in ATF-1 and extended fabrication pellets. 22
Table 5. ATF-1DU sample phase quantification measurement comparison. 23

ACRONYMS

ASTM	American Section of the International Association for Testing Materials
ATF	accident tolerant fuel
BSE	backscattered electron
CA	contamination area
CI	confidence interval
DGD	diamond grinding disk
DU	depleted uranium
EDS	energy dispersive X-Ray spectroscopy
EU	enriched uranium
ID	identification
INL	Idaho National Laboratory
LOM	light optical microscope
LWR	light water reactor
RA	relative accuracy
SD	standard deviation
SE	secondary electron
SEM	scanning electron microscope
TOPO	topographic
XRD	X-ray diffraction

Grain Size and Phase Purity Characterization of U_3Si_2 Pellet Fuel

1. INTRODUCTION

Optimization of light water reactor (LWR) fuel technology is fundamental to ensure continued economically competitive use of the existing fleet of commercial nuclear reactors. These reactors must be operated within the boundaries defined by existing fuel safety criteria, designed for UO_2. [1] As new fuel forms mature to the point of evaluation within a commercial reactor, confidence in characterization measurements and reliable characterization methods become critical. U_3Si_2 is being pursued as an optimized LWR fuel due to its higher/increasing thermal conductivity at elevated temperatures and its superior uranium loading when compared with UO_2. Many characteristics that are well understood and known to be an important quality specification for UO_2 have not been evaluated in U_3Si_2. Some characteristics relevant for UO_2 may not be as important for U_3Si_2 and vice versa.

Initial fabrication and subsequent characterization of U_3Si_2 [2] have demonstrated the difficulty in manufacturing phase pure U_3Si_2. Pellets made for initial irradiation testing at the Idaho National Laboratory (INL) were reported to be only 84-88% U_3Si_2 with secondary Si rich phases accounting for up to 13% of the mass and an oxide phase ranging from 2-4% measured via X-ray diffraction (XRD). Differing methods of fabrication have produced higher phase purity in small lab scale quantities [3], but the methods for U_3Si_2 pellet fabrication have yet to be perfected or scaled to larger production. Accurate quantification of the phase purity is a key parameter in evaluating the quality of initial batches fabricated for commercial reactor insertion as part of a lead test rodlet. The phase quantification becomes particularly important as the phase purity value may affect neutronics and other safety related modeling calculations, such as thermal conductivity and swelling.

Grain size and pore morphology may also influence pellet performance, and should be thoroughly characterized before irradiation, both to inform fabrication and to provide reference during post irradiation examination.

Characterization methods include: sample preparation, light optical microscope (LOM) and scanning electron microscope (SEM) micrograph collection, corresponding energy-dispersive X-ray spectroscopy (EDS)/XRD phase determination/verification, subsequent image analysis, and data recording. Those methods need to be sufficiently defined and controlled to provide consistent phase and grain size information in order to provide confidence in the material characterization before insertion in a reactor. This level of rigor and more is currently applied to commercially fabricated UO_2 pellets on a regular basis, but applicable methods need to be extended to U_3Si_2. This level of rigor and more is currently applied to commercially fabricated UO_2 pellets on a regular basis, but applicable methods need to be extended to U_3Si_2. An accurate pre-irradiation determination of the fuel microstructure facilitates interpretation of the irradiation-induced microstructural modifications that are likely to be observed after irradiation.

This work provides a thorough description of material characterization methods employed in the analysis of uranium silicide microstructure with corresponding measured values and interpretation. The report is organized as follows: A description of the samples characterized, and sample preparation methods that pertain to both grain size and phase measurements. Grain size measurement method is explained beginning with LOM micrograph collection and image analysis techniques to measure grain size. Phase purity measurement methods are explained beginning with SEM micrograph collection, phase identification, and image analysis techniques for phase quantification. Grain size measurements are reported with representative images and comparison of values according to fabrication batch. Results of phase identification with representative examples and explanations of unexpected phases are provided. Phase quantification measurements are reported with a comparison of phase quantities per sample.

Discussion of unidentified phases and the impact of fabrication parameters on the measurements are included.

2. MATERIALS AND METHODS

This work describes methods derived from the American Society for Testing and Materials (ASTM) standards for measuring average grain size of U_3Si_2 pellets and quantifying porosity and phases present within U_3Si_2 pellets via image analysis. The standards, ASTM E112 - 13 Standard Test Methods for Determining Average Grain Size [4] and ASTM E 1245-03 Standard Practice for Determining the Inclusion of Second Phase Constituent Content of Metals by Automatic Image Analysis [5] and standards called out within those standards [6,7], were followed to the extent possible.

Pellets used for this characterization were fabricated at INL using methods detailed by Harp et al [2]. Over sixty pellets were fabricated for evaluation and irradiation in the Advanced Test Reactor as part of the Advanced Fuels Campaign Accident Tolerant Fuel program, hereafter referred to as "ATF-1 pellets." Representative samples were selected from both a depleted uranium (DU) and enriched uranium (EU) batch. In a second phase, as part of an extended fabrication program, additional pellets were produced with optimized fabrication parameters. Those comprise: adjusted stoichiometric quantities of U and Si used to formulate the U_3Si_2 compound, a sintering environment with less O_2 impurity, and reduction of time U_3Si_2 powder was exposed to O_2 gas. The O_2 gas exposure was a result of powder storage in the argon environment fabrication glovebox where the O_2 levels were controlled to less than 5 ppm nominally. Samples from this fabrication procedure have also been characterized, hereafter referred to as the "extended fabrication pellets." The extended fabrication pellets were produced on a larger scale, nearly double compared to the ATF-1 quantity, with EU pellet samples from ten different batches[a] characterized in the present work. The later 5 batches were made with a combination of EU U_3Si_2 feedstock powder from an outside vendor combined with DU powder fabricated per processes outlined by Harp et al [2]. These later batches were also sintered in a graphite crucible lined with Ta foil, 7 pellets at a time, while the first half of extend characterization pellets were sintered in a Ta crucible, 3 pellets at a time.

2.1 Sample Preparation

2.1.1 Sectioning

Pellets were sectioned both longitudinally and radially with a high speed Struers precision saw equipped with an 8-inch diameter SiC blade rotating at 3000 - 5000 rpms. The feed rate of the pellet was set between 0.005 - 0.050 mm/second depending on the individual sample, and generally being slowed down near the end of the cut to avoid large breakaway near the edge. Pellets were secured in specially made holders to accommodate the plane of the cut. For longitudinal sectioning, the pellets were positioned at an angle to the blade to help minimize breakaway near the edges. The cut was made in roughly the center of the pellet, with great care taken to avoid misorientation along the longitudinal axis [4,5]. The longitudinally oriented specimen is preferred, as shown in Figure 1, as it provides more information about the microstructure. The longitudinal plane of the pellets is parallel to the deformation axis and allows evaluation of potential microstructural variation along the x and y planes following pellet formation pressing. Such information is not quantifiable from a single radial cross section, as only the z plane is examined in this type of cut. A longitudinal section also allows assessment of any possible elongation or compression within the sample's microstructure [4].

a A batch in this case was defined as the amount of pellets originating from one arc cast ingot of U_3Si_2 compound.

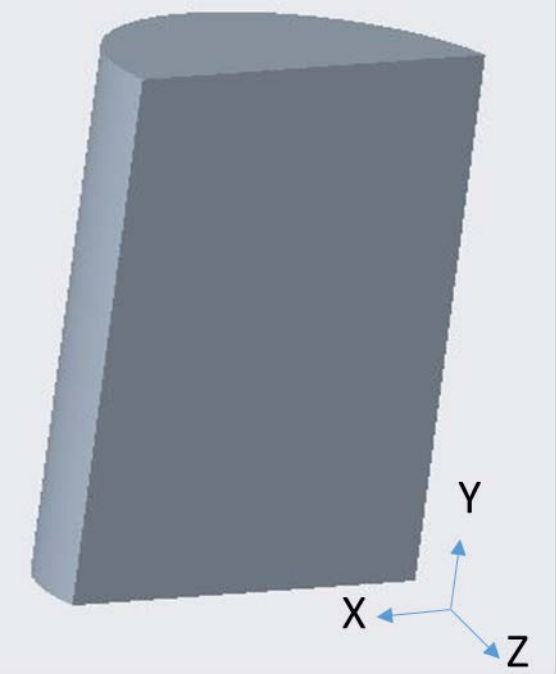

Figure 1. Longitudinal cross section representation.

ATF-1 pellets were roughly 4 mm in height, while the extended fabrication pellets were roughly 10 mm in height. The outer diameter of all the pellets was about 8 mm, resulting in a total surface area for each radial section around 50 mm^2. The longitudinal cross section surface area of the ATF-1 pellets is around 32 mm^2 and for the extended fabrication pellets is around 80 mm^2. Both ATSM E112 and ASTM 1245 suggest a minimum required polished surface area of 160 mm^2. Therefore, depending on the dimensions of future pellets, multiple pellet samples may be required for this characterization to achieve a better statistical significance. Limited samples were available for this work, and the ASTM standard recommendations were followed to the extent possible.

2.1.2 Mounting

While the standards do not require samples to be mounted, they do indicate that an unmounted sample requires a much greater polished surface area than a mounted sample. In addition to limited sample surface area availability, U_3Si_2 pellet sections are much easier to polish and handle when they are mounted. Pellet sections were mounted by sticking the flat edge of the sample on a piece of electric tape and centering a plastic ring form around it on the tape. Beuhler EpoThin 2 mounting epoxy was then poured over to cover the sample and allowed to harden.

2.1.3 Polishing

A general guideline for polishing epoxy mounted U_3Si_2 on a Buehler AutoMet automatic polisher within a polishing “contamination area” (CA) enclosure using a combination of successively smaller diamond grinding disks (DGD) and polycrystalline diamond suspensions has been developed. The standard steps are listed in Table 1.

Table 1. General guideline for polishing epoxy mounted U_3Si_2.

Step	Polishing media size (µm)	Polishing cloth	Force (pounds)	Rotation speed (rpms)	Rotation direction	Duration (min.)
1	75 diamond	DGD	4-5	150-180	Comp. (same)	2-10
2	55 diamond	DGD	4-5	150-180	Comp. (same)	2-4
3	35 diamond	DGD	4-5	150-180	Comp. (same)	2-4
4	15 diamond suspension	Struers MD Dac	3-5	140-180	Comp. (same)	2-10
5	9 diamond suspension	Buehler VerduTex	3-5	140-180	Comp. (same)	2-10
6	3 diamond paste	Beuhler Trident	3-5	140-180	Comp. (same)	2-10
7	1 diamond suspension	Beuhler MasterTex	3-5	140-180	Comp. (same)	0.5-1

However, often the polishing procedure is unique to the specific sample and is affected by sample characteristics such as density and grain size. The typical procedure begins with a 75 µm DGD for 2-10 minutes, depending on how long it takes to get the mounted surface flat. To ensure the sample is flattened, the met mount is initially colored with a black permanent marker and is considered flat when the marker has been entirely removed across the face of the mount. The same parameters are used in the next steps stepping down through to the 55 and 35 µm DGDs for about 2-4 minutes at each step, depending on when the sample appears to have lost all the deformations, i.e., scratches and pullout from the previous step. The progress of the sample between steps can be observed with the naked eye to some extent. The sample surface becomes shinier as it gets more flat and smooth or dull as a result of pullout across the sample. A Dino-Lite portable microscope with up to 200x magnification was used inside the polishing CA enclosure connected to a laptop display outside the CA to keep a closer observation of sample preparation progress. This also provides a better qualitative idea of what the sample should look like to the naked eye after each step.

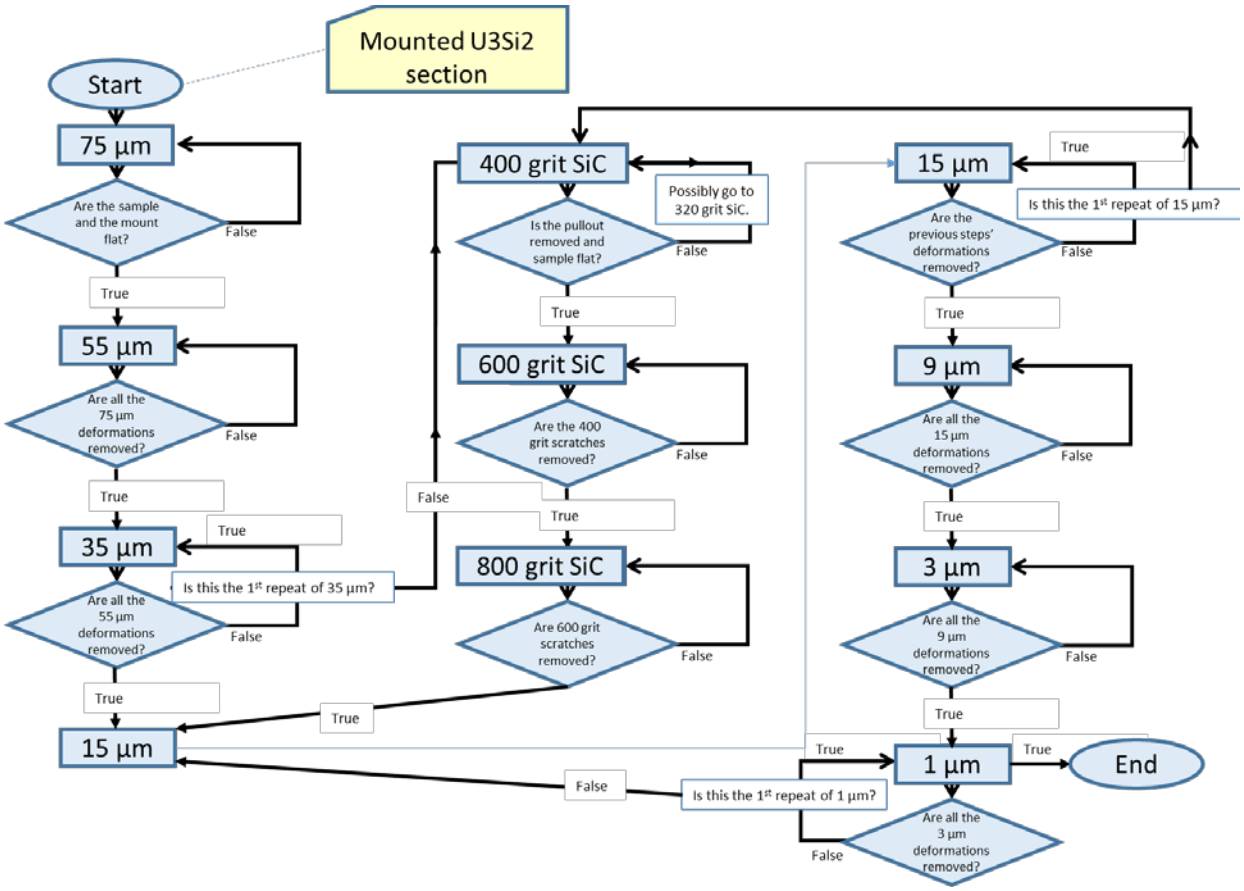

Figure 2. Polishing steps for a mounted U_3Si_2 pellet section.

Because U_3Si_2 has characteristics of both a metal and a ceramic, it can be challenging to polish because it is susceptible to both scratches (characteristic of a metal) and pullout (characteristic of a ceramic). Depending on the sample, pullout induced in these early steps cannot be removed in subsequent steps, and alternate approaches may be required. A flow chart, Figure 2 illustrates the general procedure and most variations. After the 35 µm DGD step, if the sample is starting to look a little shinier and less scratched, the next progression involves the diamond suspensions, starting with 15 µm through to 1 µm, checking the sample every 1-2 minutes with the Dino-Lite to ensure the sample appearance is improving or has removed the previous step's deformations. In some samples, the 1 µm step does more harm than good, so extra precaution is taken at that step to check progress every 30 seconds. 30 - 60 seconds is generally long enough to remove the 3 µm scratches. After any of the above listed steps, if the sample appears worse than it did before that step, it could be a result of carryover from the previous step due to inadequate cleaning between steps, or due to a unique characteristic of that specific sample. Either way, it is necessary to go back a few steps and/or start over. In the case of pullout getting worse until the sample becomes dull, SiC grinding disks starting between 400-800 grit and successively polishing up to 800 grit may be employed before going back to diamond polishing media at the 15 µm diamond suspension step.

2.2 Grain Size Analysis

After a satisfactory 1 µm finish has been achieved, the samples are ready for optical microscopy to measure average grain size. The linear intercept procedure [4] is used to measure average grains size in UO_2 fuel pellets and has been adapted for use on U_3Si_2 pellets. The intercept method involves an actual count of the number of grains intercepted by a test line or the number of grain boundary intersections with a test line, per unit length of a test line, used to calculate the mean linear intercept length, l_m. [4]

2.2.1 Collecting LOM Images

An inverted Zeiss LOM (Observer.D1m) with a polarizing lens reveals the U_3Si_2 pellet grain structure without the use of chemical etchants. The images produced with polarized light exhibit grain contrast of color differences between the grains rather than the grain boundary delineation that is enhanced by enchants. [6]The microscope is adjusted to evenly illuminate the field of view, and the focusing knob is oscillated between under focus and over focus in successively smaller increments until the image is sharp. [7] The image illumination and focus are adversely affected if the sample surface is not completely flat. In this case, a portion of the location where the measurement can be achieved is optimized. The microscope is equipped with built-in photographic capabilities, and the enlarged sample view is delivered to a computer monitor [7]. A stage micrometer is photographed each day measurements are taken, at the range of magnifications utilized, to determine the true linear magnification. Photomicrographs are made at a range of magnifications: 25x-50x are typically employed to capture a montage of the entire sample surface, and later stitched together using Adobe Photoshop; 100x - 1000x are used to capture micrographs for grains size measurements depending on the size of the grains. Higher magnifications are used to provide more information about any unique features within a sample. To determine the appropriate magnification for grain size measurements, the magnification is adjusted until the smallest grain on the photomicrograph is about 5 µm and at least 50 grains are observed within the measurement area. [6] Typical average grain diameter of U_3Si_2 pellet specimens range from around 15 - 40 µm depending on processing parameters. For that range of grain size, a 200x magnification achieves an appropriate amount of grains per area for the measurement.

Between 5 and 25 micrographs are taken across the sample surface in differing locations to achieve adequate statistical significance. The micrograph image file name includes the sample's unique ID, the plane at which the image was collected, i.e., radial or longitudinal, the magnification, and a reference to the number of images taken per sample (Ex: 1108rad200x1). Depending on specific program requirements, more micrographs may be necessary. To avoid bias in the measurement, the x and y stage controls are moved without looking at the screen with care to not overlap measurement fields and avoid choosing "typical" or "worst" fields [6]. Sample preparation induced pullout and damage will be visible across the sample surface, more or less depending on the specific sample and skill of sample preparation personnel. These areas must be avoided, as the grains are not adequately defined in areas with excessive pullout or damage.

2.2.2 Intercept Method

The average grain size is estimated by counting, on a photomicrograph of a representative field of the specimen, the number of grains intercepted by a circular test line with sufficient radius to yield at least 35 intercepts, as recommended by the standard. [4] An intercept is defined as a segment of a test line overlaying one grain. An intersection is defined as a point where a test line is cut by a grain boundary. Either may be counted, with identical results in single phase material. U_3Si_2 pellets measured are not single phase, and have a UO_2 phase that is visible in the optical micrographs, but is ignored in the determination of grain size. The circular intercept method was chosen because it automatically compensates for departures from equiaxed grain shapes without overweighting any portion of the field, and avoids the ambiguous intersections at the ends of test lines associated with the lineal intercept method. [4] The circular method is well suited for fixed routine manual procedures for grain size estimation in quality control. [4] An example of this method applied to U_3Si_2 pellets is shown in Figure 3.

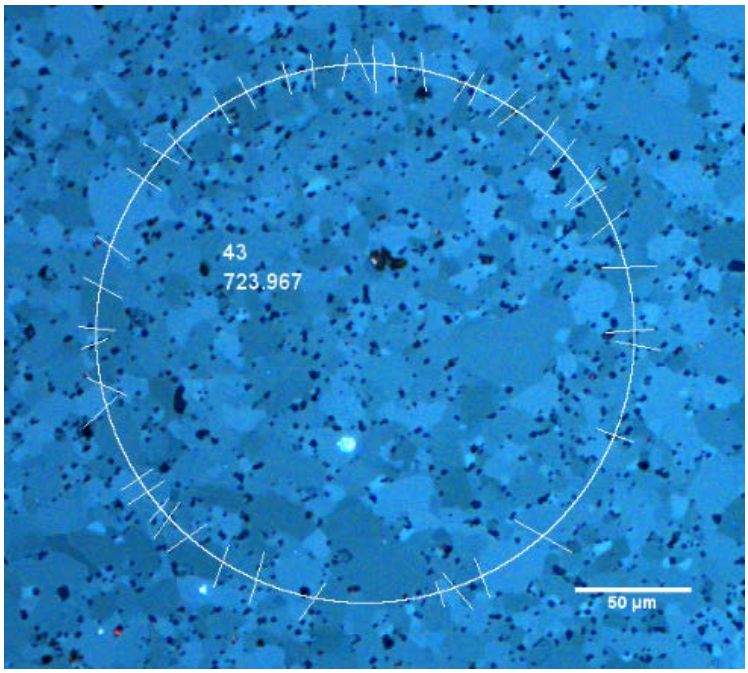

Figure 3. An example of a polarized optical micrograph (1005200xlon.tif) with the circular intercept grain size determination method illustrated.

The micrographs of the sample are opened in the Image-J software program along with the corresponding magnified image of the scale bar, which is used to set the global scale within the software that applies to all images opened within that session. One circle per field of view is applied blindly over as large a specimen area as feasible with the precision increasing with more counts per circle. The perimeter of the circle is measured and recorded in an excel file and typed on the image. The grain boundaries intercepting the circle are drawn over with a pencil tool in the software and counted. The number of intercepts is recorded in the previously mentioned excel file and typed onto the image as well. The analyzed image is then saved into a "grain size analysis" folder unique to the sample for future reference. Bias in the measurement can be introduced at this step when the grains are not clearly delineated, and some judgement is required in drawing where the grain boundaries are. If an outlier in measurement is observed, or for auditing purposes, the saved images can be consulted for errors such as a mistake in counting the intersections or setting the scale.

The standards recommend a total of at least 500 grain boundary interceptions, which translates to roughly 14 photomicrographs per specimen. For the present measurements, 5 fields of view were used with roughly 35 intersections measured per micrograph equating to roughly 175 counts per sample. Precision increases with intercept counts, so more micrographs may be required for future measurements.

The radial intercept length, l, for each field, n, is calculated by dividing the circumference (total test line length, l_c) by the number of intercepts counted, i. Then, the mean radial intercept length, l_m, is calculated by dividing the mean of the circumferences from each field, l_c, by the mean of the intercepts counted from each field, i. The equations for standard deviation (SD), 95% Confidence Interval (CI), and Relative Accuracy (RA) found in the standards [4, 5] are calculated for each l_m measurement with the intent of reaching an RA of 10% or lower.

2.3 Phase Purity and Porosity Analysis

2.3.1 Collecting SEM Images

After a sample has been examined with the LOM, it can be coated in preparation for SEM examination, which is required for the phase purity measurement. Gold coating is a standard procedure used to avoid charging on the sample surface. The coated sample is secured to the SEM fixture with copper tape to further inhibit charging affects. The SEMs used for this work include a JEOL 7600 and a Phenom XL set to an operating voltage of 20 kV and 15 kV, respectively, each equipped with a backscattered electron (BSE) detector and EDS. The JEOL has a secondary electron (SE) detector that provides topographic information about the sample surface while the Phenom has a topographic (TOPO) mode that provides similar information.

The working distance of the JEOL is set to 8mm. The working distance for the Phenom is set when loading the sample by the displacement of the of the sample holder platform. The sample is secured to the base of the holder, the holder is adjusted to bring the surface of the sample to be flush with the top plane of the holder, and then moved down 8 spaces with the adjustment wheel.

The measurement of phase purity and porosity of U_3Si_2 pellets is performed by collecting SEM images that contain discrete secondary phases and porosity. These features are detected, discriminated, and quantified based on their grey level intensity differences compared to each other and the matrix.

Table 2. Parameters used in collecting micrographs.

Microscope	Detectors	Magnification	Voltage
JEOL 7600	BSE, SEI	Pores: 250, Phases: 1000X-2000X	20 kV
Phenom XL	BSE, TOPO	Pores: 1000X, Phases: 3500X	15 kV

In order to consistently discriminate between pores and secondary phases from sample to sample, the settings for each microscope were replicated for each exam and are listed in Table 2. To discriminate voids from dark phases within the sample, duplicate images are taken with both the BSE and SE/TOPO. Figure 4 provides an example of the resultant micrographs from each microscope and setting. The lower magnification (250X for the JEOL and 1000X for the Phenom) used to measure pores allows measurement of a greater area. This increases the statistical significance and avoids error from edge effects that becomes more important at higher magnifications. The higher magnification, used to measure phases, allows appropriate resolution to identify all present phases within the sample.

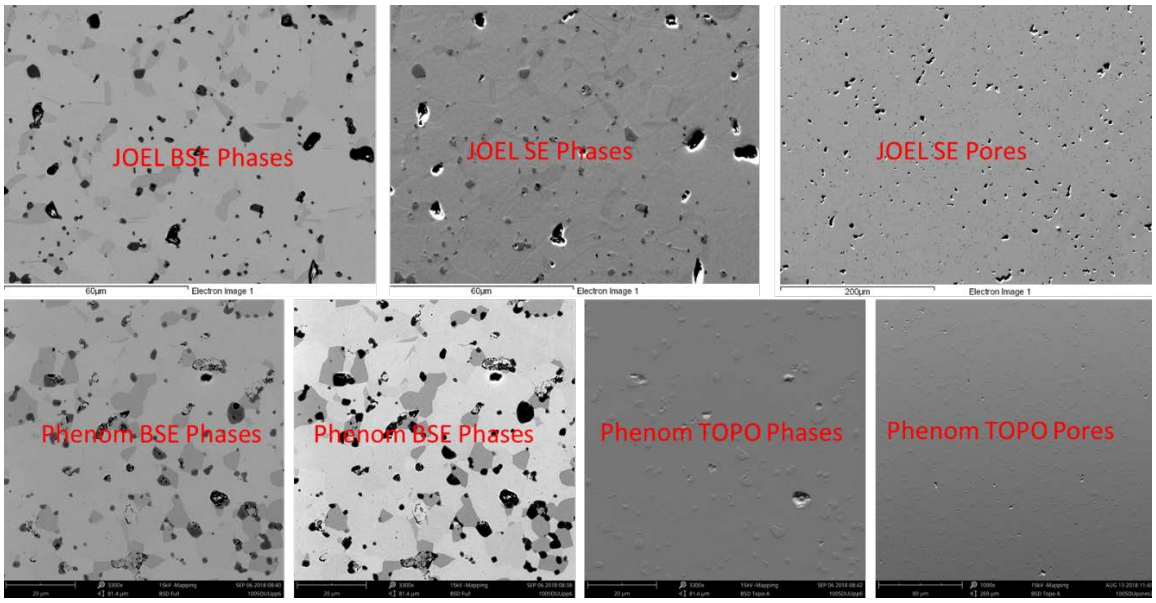

Figure 4. Example of micrographs from both the JEOL 7600 (top row) and the Phenom XL (bottom row) at differing magnifications to measure phases with higher magnification (left side) and pores with larger area (right side).

For phase measurements, the brightness and contrast were adjusted to maximize the contrast between all the different phases. Although slightly different magnifications were used between samples, for each sample, a consistent magnification was used for each field of view/micrograph used to calculate the average value. Five fields of view were collected per sample, with an additional five fields of view at the higher magnification for phase measurements with a micrograph collected in both BSE and SE/TOPO mode. Similar to the LOM micrograph collection for grains size, the fields of view were randomly selected to avoid bias and overlapping.

Grey-level thresholding on the BSE image is used to discriminate pores when measuring phases. Porosity discrimination is accomplished by comparing a SE/TOPO image in the same location as the BSE image to verify voids within the sample. Some lighter Z number element phases such as oxides appear darker and can be confused with voids, depending on the brightness and contrast setting on the SEM. Pores are typically found within oxide phases; however, since an iron-containing phase can look like porosity, the SE/TOPO images are important to verify location of voids, as shown in Figure 3. Determining if voids are actually: 1) porosity from sample fabrication or 2) preparation-induced pullout, is less straightforward. Generally, pores are more rounded, shallow, smooth, and smaller than pullout. Some examples are provided in Figure 5.

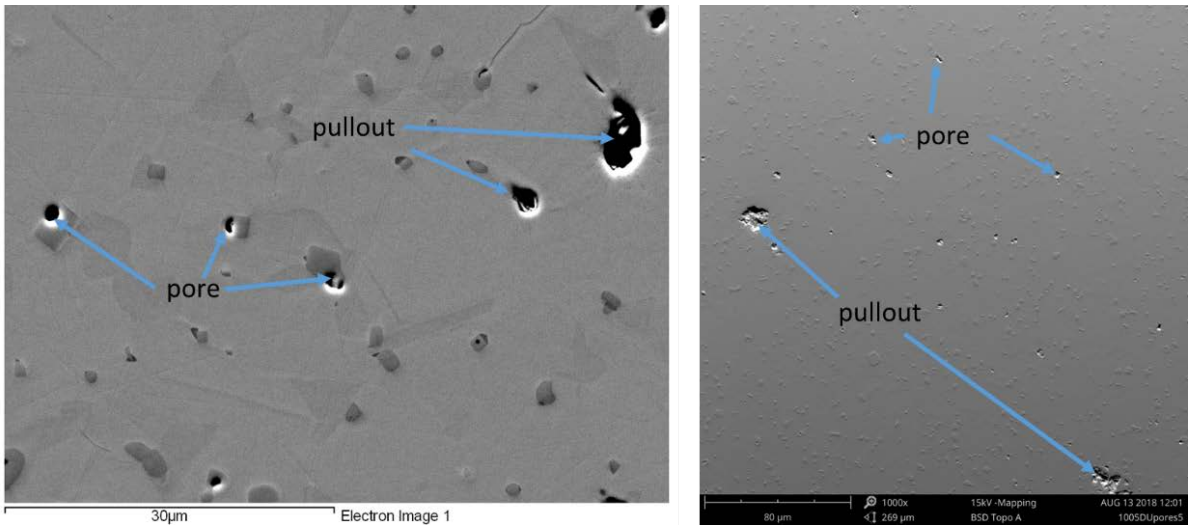

Figure 5. Examples of preparation induced pullout and as-fabricated pores.

2.3.2 Identifying Phases

To identify phases within the samples, a representative field of view was selected for EDS. The EDS technique alone is only a semi-quantitative technique and cannot positively identify phases. X-ray diffraction is also used to confirm the presence of any particular phase. Three to five point spectra were gathered on each differing grey level feature within the micrograph with a count time set to 30 seconds on each point. Because higher Z number elements appear brighter in BSE micrographs, the main phase, U_3Si_2, is the lightest phase, as it contains the most uranium of the phases observed. Other typical secondary phases include Si rich phases that appear darker relative to the amount of Si, and the dark grey phase is UO_2. As characterization has progressed, additional phases that were initially overlooked have been identified. Two different Si rich phases have been identified [9] as well as phases containing Fe, Cu, and W, as a result of fabrication methods [2, 10] and U_3Si_2 feedstock contamination. Examples of these elements within U_3Si_2 are shown in Figure 6.

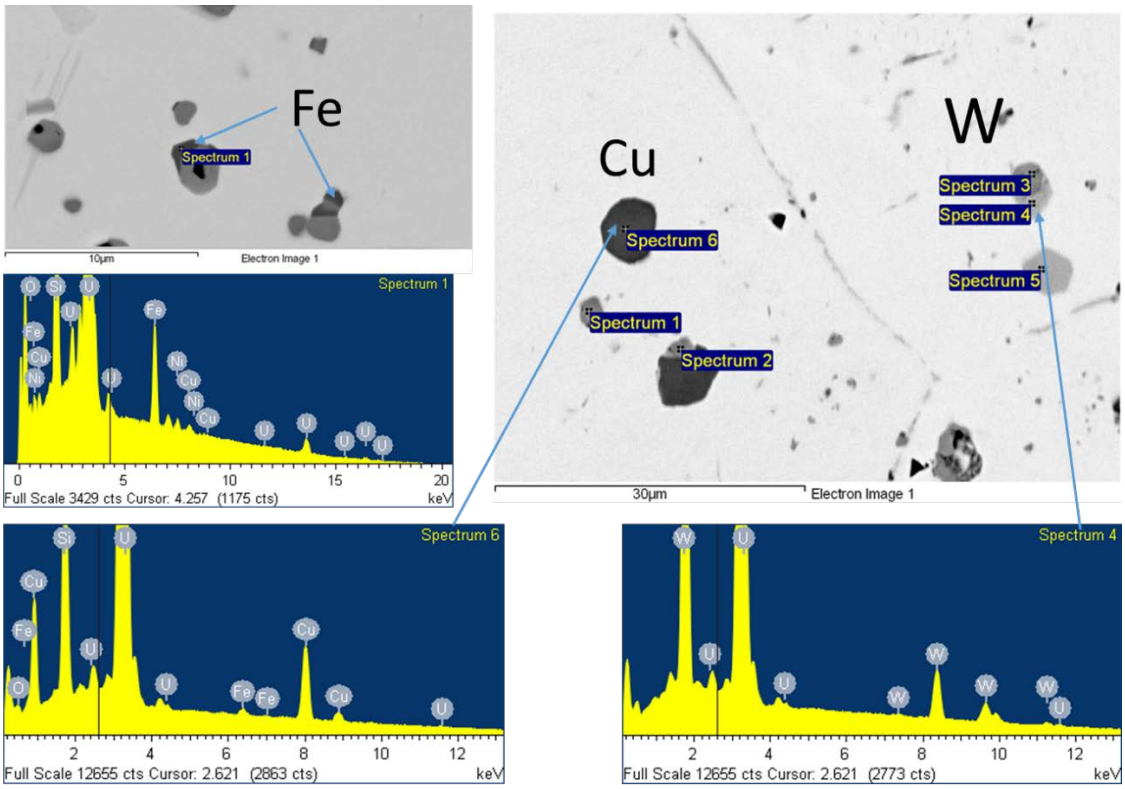

Figure 6. Examples of miniscule phase impurities containing Fe, Cu, and W in a U_3Si_2 pellet sample.

Copper present in samples is attributed to excess material contact with the arc-melter copper hearth when pressed U-Si powder compacts were melted before adding the process step of agglomerating. [2] Copper was only observed in ATF-1 development samples before that process change was implemented. Tungsten is also attributed to the arc melting step where a tungsten electrode is used to melt U and Si, forming U_3Si_2.

Iron is a common contaminant in uranium. The iron containing phases within the U_3Si_2 pellets likely originate in the U feedstock. Chemical analysis of the U feedstock confirms elevated levels of iron. The iron phase, shown in the top left of Figure 6, is small relative to other features in the U_3Si_2 pellet, and is generally observed as a darker feature connected to a UO_2 phase or at triple point of grain boundaries. A larger magnification is required for the point spectra on the iron phase. A line scan is also employed for some regions too small for a point to simply verify the existence of iron in the region.

A map of the representative field of view is also very useful, especially in segregating the Si rich phases, as their grey-level threshold is very close, their Si content difference in a mapped image provides a better illustration, Figure 7. Mapping capabilities on the Phenom XL SEM are very low resolution, and use of the JEOL 7600 for this work was limited, so mapping was not done for most of these measurements.

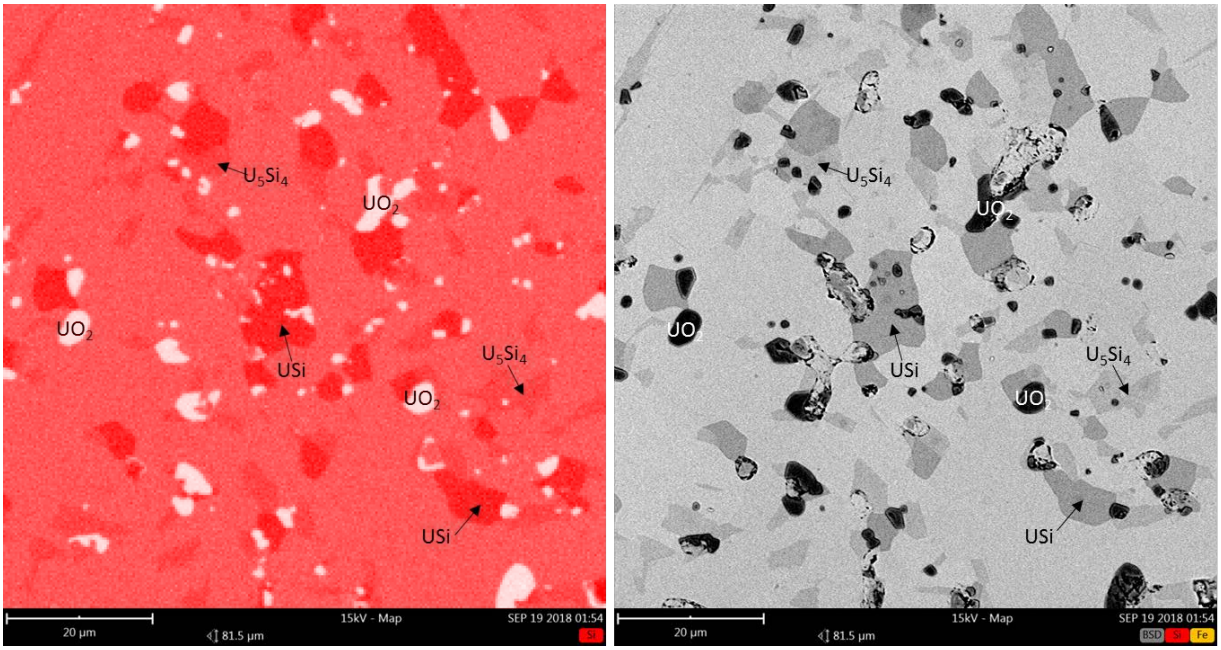

Figure 7. Silicon elemental EDS map of an ATF-1 DU sample and corresponding SEM BSE micrograph.

In addition to the EDS phase identification method described above, XRD phase identification was completed on most of the samples and agreed nicely with the EDS measurements. The resolution and refinement of the crystal structure of compounds is generally an adequate method to determine sample composition. However, because of the large difference between the scattering power of the heavy (U) and the lighter atoms (Si, C, Fe, etc.), a large uncertainty is considered concerning the lighter element phases. [10] Because the expected quantity of some phases is so low, close to the detection limit for the XRD measurement method, phase quantification was not as accurate as with image analysis. The phase quantification from XRD did report the levels of UO_2 in samples in agreement with image analysis measurements.

Future methods may include use of Electron Probe Microanalysis on a select representative sample or use of fabricated U-Si phase standards to verify SEM EDS.

2.3.3 Image Analysis

Figure 8 shows a BSE and SE image for the same location on a typical U_3Si_2 sample with corresponding image thresholding. Here the Si rich phase is calculated as one phase.

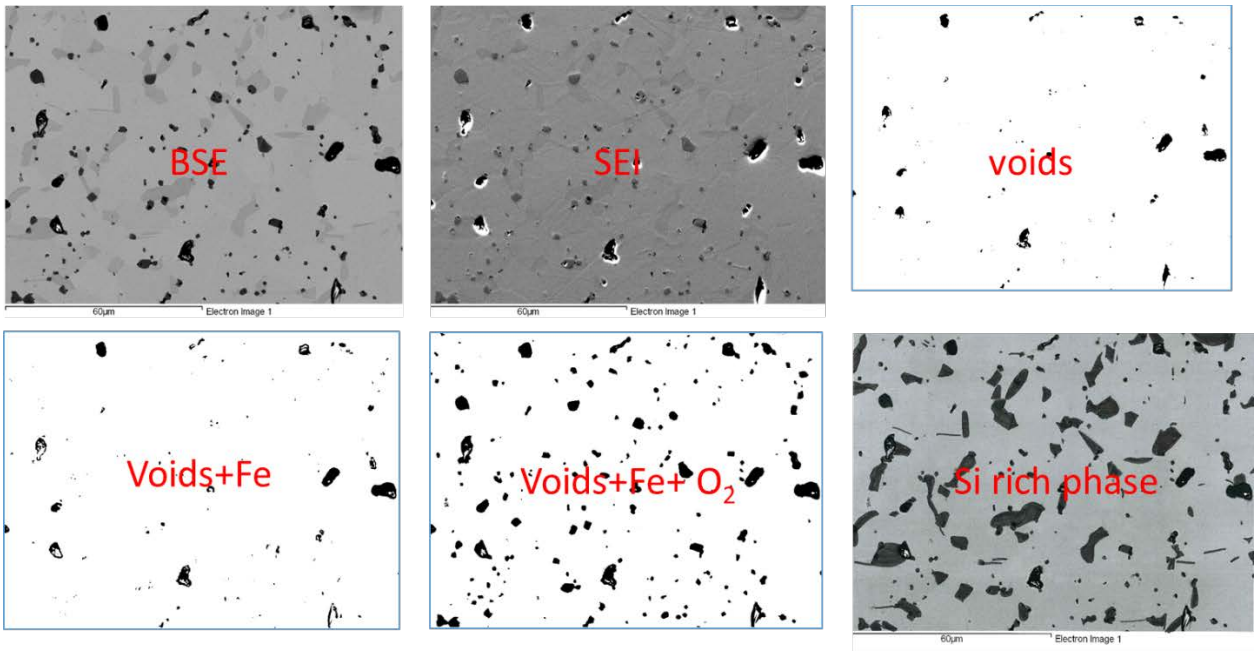

Figure 8. BSE, SEI, and corresponding duplicated BSE images adjusted to segregate individual phases.

For grey level thresholding and quantification, SEM BSE micrographs are opened in Image-J software. The micrograph image file is labeled with the unique sample identification, the letters PP or PORES indicating what measurement the image was collected for, and the field of view numbered one through n (Ex: ID 1405PP3, for the third field of view on the Sample ID 1405 for phase purity measurement). The scale bar included on the SEM micrographs is used to set the global scale within the software. An outline of the entire image, excluding the scale bar or other data, is selected and cropped. That area, the total area of the particular field of view, is measured and recorded in an excel file. Then the cropped image is duplicated one time for each phase present in the sample.

The first inclusion measured are the voids: composed of fabrication-induced porosity and sample preparation-induced pullout. Pullout and porosity are not easily/quickly distinguished, making the avoidance of pullout important, specifically in sample preparation and to the extent possible in collecting micrographs. When pullout locations within a micrograph area are not subtracted from the total area, it skews the total area of examination, thereby skewing all measured values. The image threshold is adjusted to highlight only the darkest features (the voids), and, once applied, all other features are removed from the image. Then, the area fraction of that feature is computed, and the value is manually recorded into an excel spreadsheet. The adjusted image is saved with the original file name plus the phase measured (Ex: ID405PP3voids).

The next darkest feature is the iron-containing phase, so the threshold on an unadjusted duplicated image is adjusted to highlight both the voids and iron phase. The area of the combined voids and iron phase is computed and entered into the excel spreadsheet. Then the adjusted image is saved as the original file name plus voids plus Fe (Ex: ID405PP3voids+Fe).

The UO_2 phase is distinguished because of its darker color relative to the matrix. The threshold on an unadjusted duplicated image is adjusted to highlight all the voids, iron phase, and the UO_2.The area fraction is calculated and recorded in the same way as the previous phases.

The Si rich phases, USi and U_5Si_4, are somewhat less straightforward to threshold, shown in Figures 7, 8, and 10, due to shading effects across the image. For example, a USi phase on the left side of a field of view will be the same grey level as the matrix on the right side of the field. An outline of the phase quantification process is provided in Figure 9, illustrating the extra process steps required to quantify the Si rich phase(s). Representative adjusted images are provided in Figure 9.

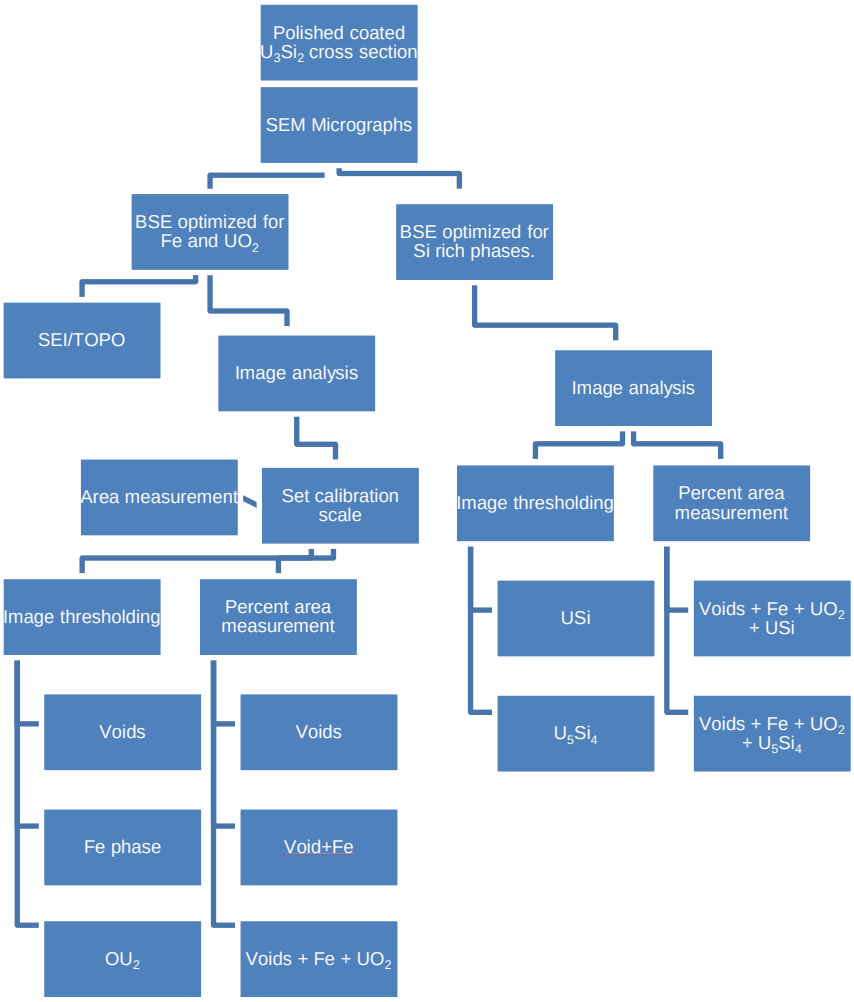

Figure 9. Phase quantification image analysis process flow chart.

Additionally complicating the Si rich phase segregation is the differing matrix contrast created by grain orientation causing a slight grey-level variation across the matrix. The best method to segregate the Si rich phases begins when collecting images. For each field of view, an additional BSE image is captured that optimizes the USi phases and makes the matrix one uniform grey level. This is illustrated in Figure 4 with the two BSE images (bottom left) shaded differently to optimize the contrast of specific phases. This also may be achieved by adjusting the SEM tilt to avoid grain contrast. Unfortunately, for most of the measurements presented here, limited SEM availability did not allow to re-obtain optimized images, so the USi phase was manually colored with a black marker on a printout of the micrograph, as shown in Figure 9. The colored images are scanned and opened in the Image-J software for analysis. All adjusted images for each field of view, such as those in Figure 10, are saved for future reference for similar reasons mentioned for saving grain size measurement images.

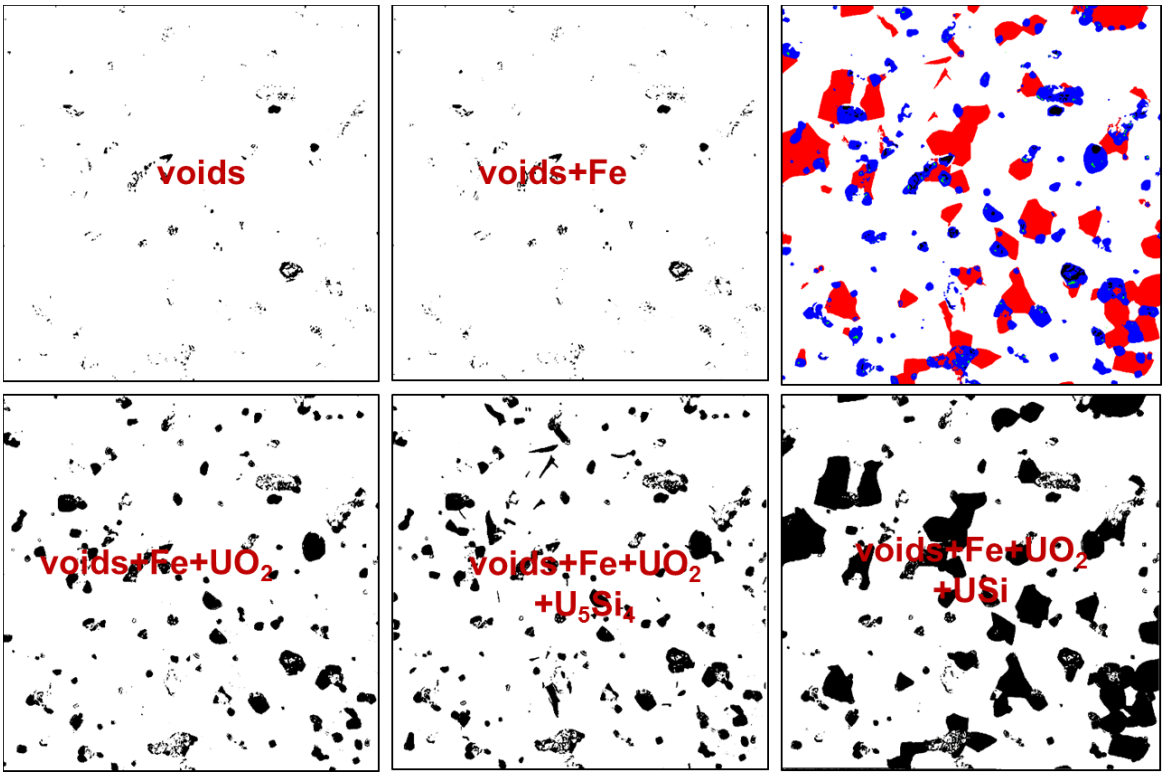

Figure 10. Grey level/phase segregation via manual and automatic image analysis shown in black and white images and the colored image (White = U_3Si_2, Red = Si rich phase, Blue = UO_2, Black = pores, Green = Fe phase) respectively.

The computed value reported in Image-J is set to area percent. Under the assumption that the phases of interest are randomly distributed in the matrix, area percent measurements are equal to volume percent. [8] The value of each phase is calculated by subtracting the Image-J measurement of all the darker phases and porosity from the phase of interest. For example, the value for UO_2 content in volume percent is given by the Image-J measurement of the adjusted image containing UO_2, iron phase, and voids minus the measurement from the adjusted image containing the iron phase and voids. Likewise, the value for U_3Si_2 is then calculated by subtracting from 100% all phases and secondary constituents measured, i.e., assuming everything else not measured is U_3Si_2.

Bias in the manual method is introduced every time an image is manually adjusted. Personal judgment is required to determine the level of thresholding. As the ASTM standard [5] notes, the threshold limits are set for the individual phases so that they are detected without enlargement of the larger inclusions. In some instances, the threshold settings may require a minor compromise between detection of the smallest and largest inclusions. The bias is mitigated by keeping the personnel completing the measurement consistent throughout a sample set.

2.3.4 Automatic Image Analysis

An algorithm in Mat-Lab® has also been developed as part of a parallel effort to quantify phase purity in irradiated U_3Si_2 pellet samples using optical images. This algorithm was modified for the SEM micrographs collected in this work and applied to the ATF-1 pellet samples to provide a comparison between the “automated” and “manual” image analysis methods. Image analysis using this automatic method is shown in the colored (top right) image in Figure 10. A graphic representation of the automated process is provided in Figure 11.

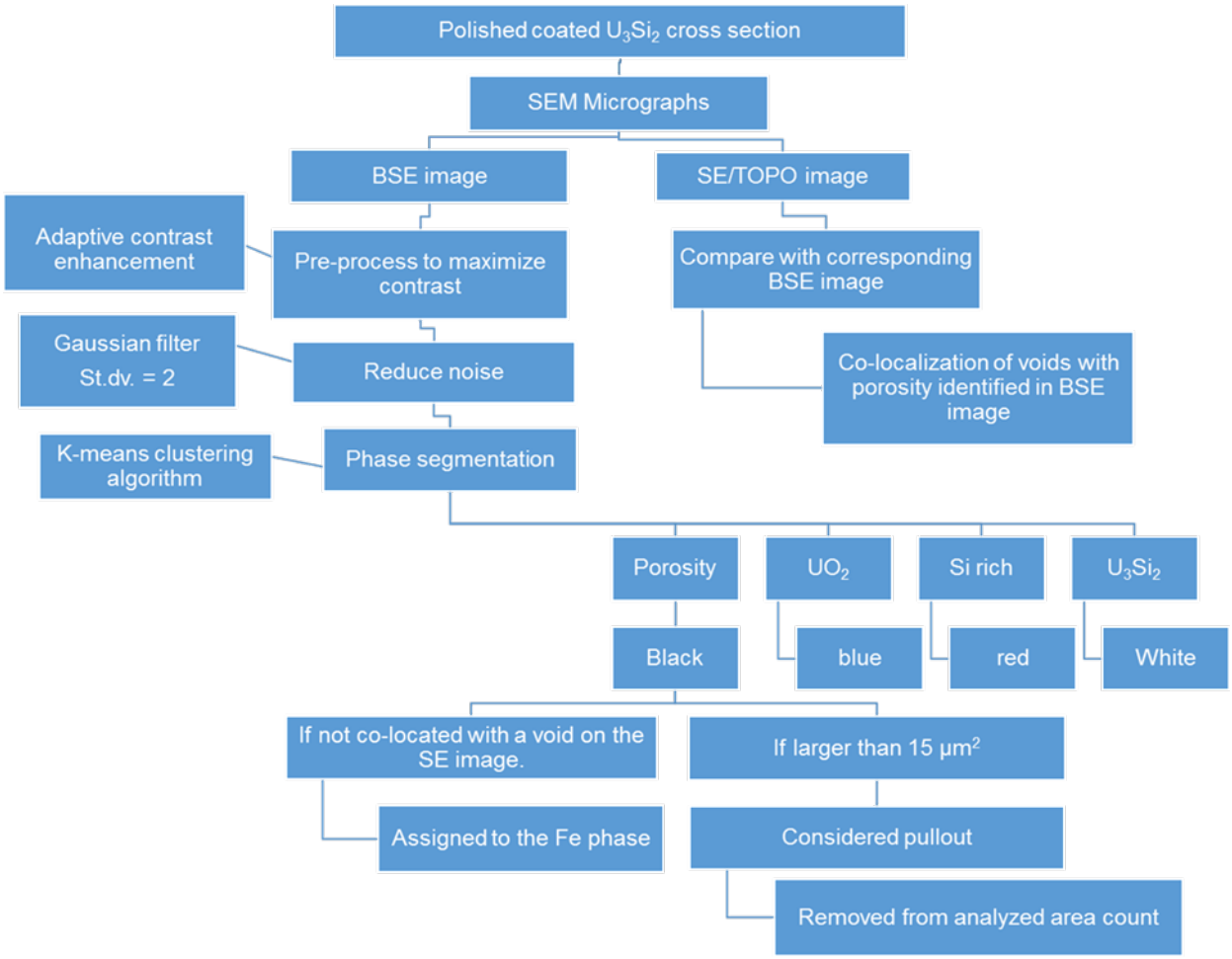

Figure 11. Graphic representation of U_3Si_2 SEM image automatic analysis.

Each collected SEM BSE image is initially pre-processed to maximize the contrast between phases using an adaptive contrast enhancement algorithm. [11] Subsequently, a Gaussian filter with standard deviation equal to two is applied to reduce the Poisson noise of the BSE image. Following the pre-processing, the segmentation is carried out using a k-means clustering algorithm, assuming the existence of four phases, namely: porosity (black phase in Figure 10), UO_2 (blue phase in Figure 10), Si-rich precipitates (red phase in Figure 10) and U_3Si_2 (white phase in Figure 10). The iron phase is discriminated by analyzing the SE images and comparing them with the BSE image corresponding to the same area, as shown in Figure 12. For each object initially assigned to the porosity phase, a co-localization with the voids identified in the SE image is evaluated: if the object in the black phase is not co-located with a void in the SE image, it is assigned to the Fe phase (green in Figure 10) and removed from the porosity count. Pullout is also accounted for by segregation from pores based on size discrimination (i.e., if an object identified as pore exceeds a pre-determined size threshold, it is removed from the porosity) and removal from the analyzed area count.

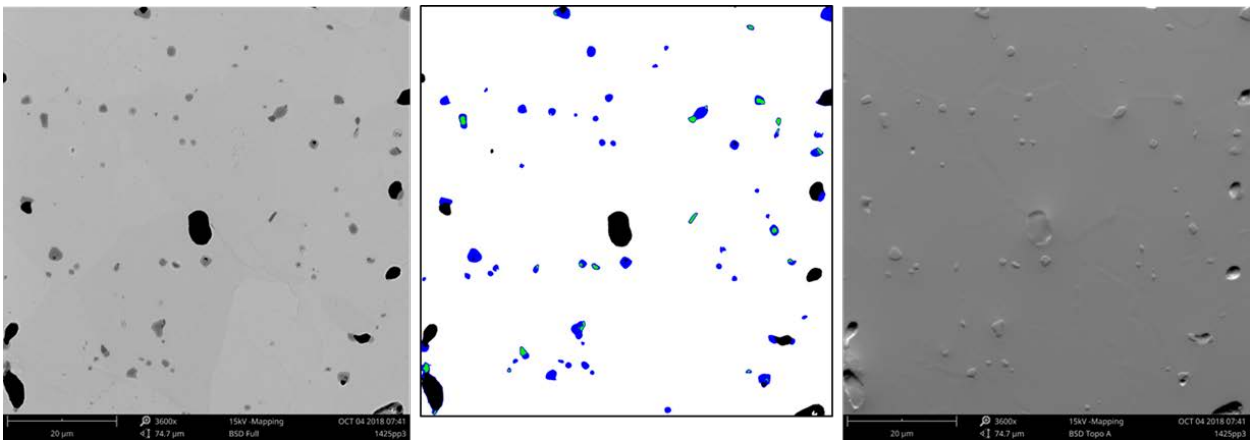

Figure 12. BSE and TOPO micrographs with corresponding grey level/phase segregation via automatic image analysis. (White = U_3Si_2, Blue = UO_2, Black = pores, Green = Fe phase).

3. RESULTS

3.1 Grain Size

Large variability in grain size was observed among the pellets, related to differing fabrication processes, especially sintering parameters. The difference in sintering environment has been discussed [2,9] where it was generally observed that sintering in a vacuum environment as opposed to an argon environment produced a denser pellet, and grains sintered in vacuum tend to be larger than grains sintered in argon. Smaller grain size for samples sintered in argon was attributed to a shorter cooling time in the argon because of the available argon atoms to carry heat away from the sample. Here pellets fabricated with a range of parameters have been measured from initial development batch pellets for ATF-1 through extended fabrication pellets that were produced in higher quantities with pellets from the second half of extended fabrication exhibiting irregular grain growth.

The average grain sizes for pellets included in the ATF-1 irradiation were the smallest of any previous or subsequent batches at ~17 µm, shown in Figure 13.

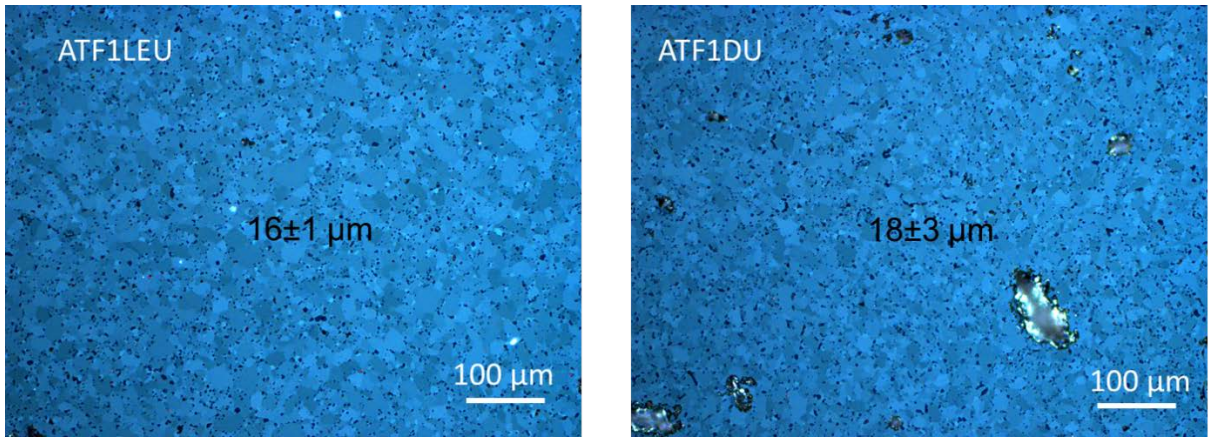

Figure 13. Representative grains of DU and LEU pellets fabricated for ATF-1.

Individual sample measurements are reported in Table 3, and Figure 14. Appendix A includes further information regarding the specific fabrication parameters, test methods used, raw data, data collection, and calculation methods.

Table 3. Grain size values for samples from ATF-1 and extended fabrication pellet samples.

Grain Size	
Batch ID	Average in µm
ATF-1DU	18±3
ATF-1LEU	16±1
1270	30±4
1301	27±2
1336	25±4
1405	25±4
1425	29±2
1437	28±3,107±11
1459	20,668,63
1476	29±4
1496	36±6,80±21

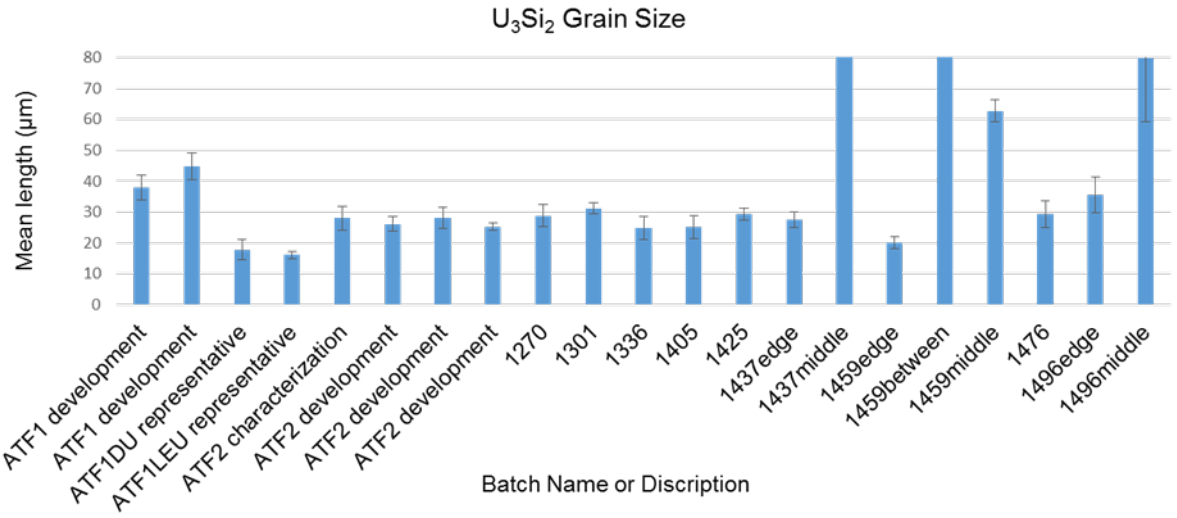

Figure 14. Grain size measurement summary for representative pellets from ATF-1 and batch samples from extended fabrication pellets.

Excluding the latter half of the extended fabrication pellets with the irregular grain growth and initial development pellets, grains sizes were relatively uniform, generally between 20 and 30 µm. This typical grain structure is shown in Figure 15.

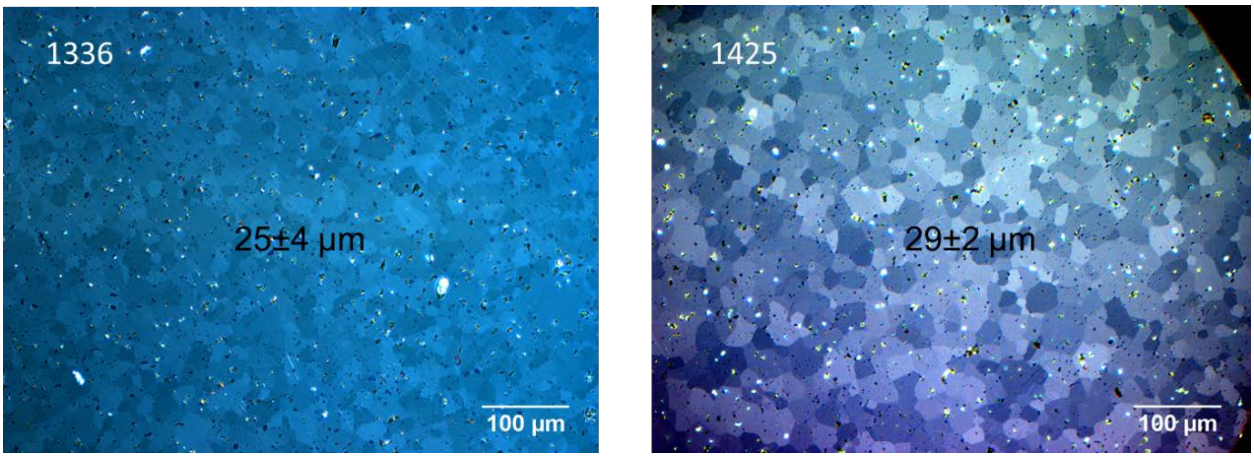

Figure 15. Representative examples of U_3Si_2 grain size.

Samples with grains larger than 80 µm were observed to have bimodal grain size distributions. All samples greater in identification number and including Sample 1437 had a finer grain structure around the edge of the pellet with a courser grain size toward the center, as indicated in the Figure 14 where some samples have multiple grain size values reported relative to location in the sample. Examples of this are shown in Figure 16 for Sample 1437 and Figure 17 for Sample 1496. The largest grains were observed in pellets sintered in the latter half of extended fabrication pellet production (i.e., after Batch 1437). Several fabrication process parameters were changed at the onset of irregular grain growth, as described in Section 2. The measured grain size values are reported here with no attempt to explain the cause of irregular grain growth.

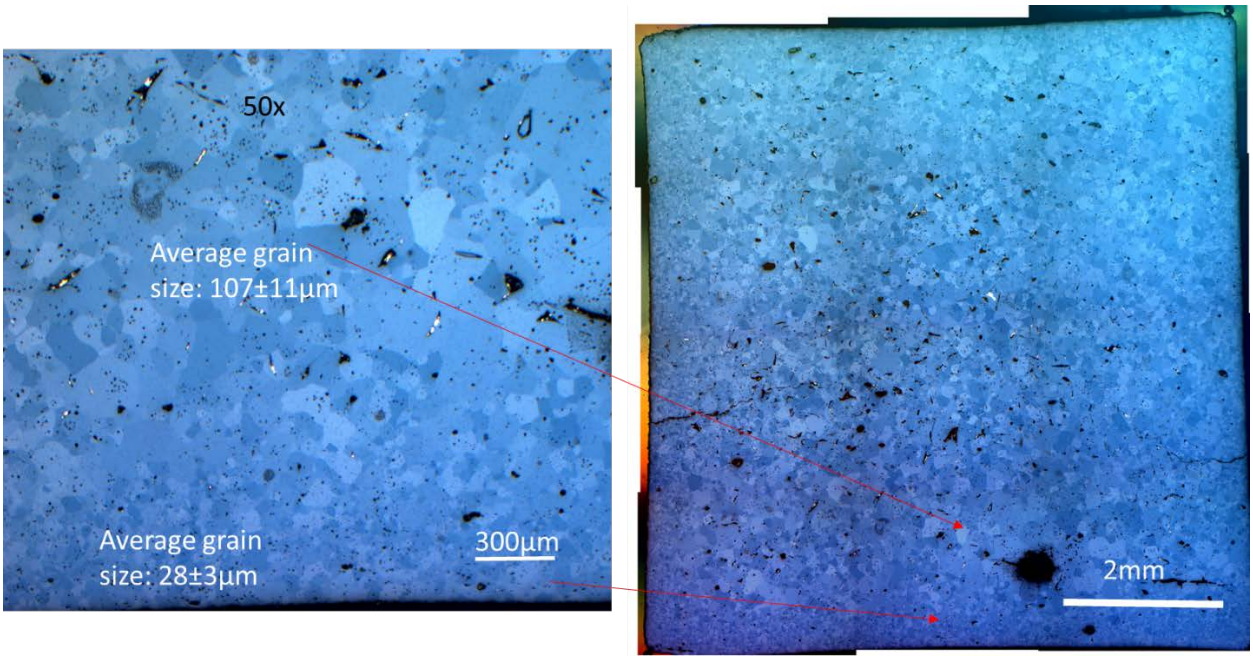

Figure 16. Longitudinal cross section of Sample 1437: example of bimodal grain growth with a coarse inner structure and fine outer structure.

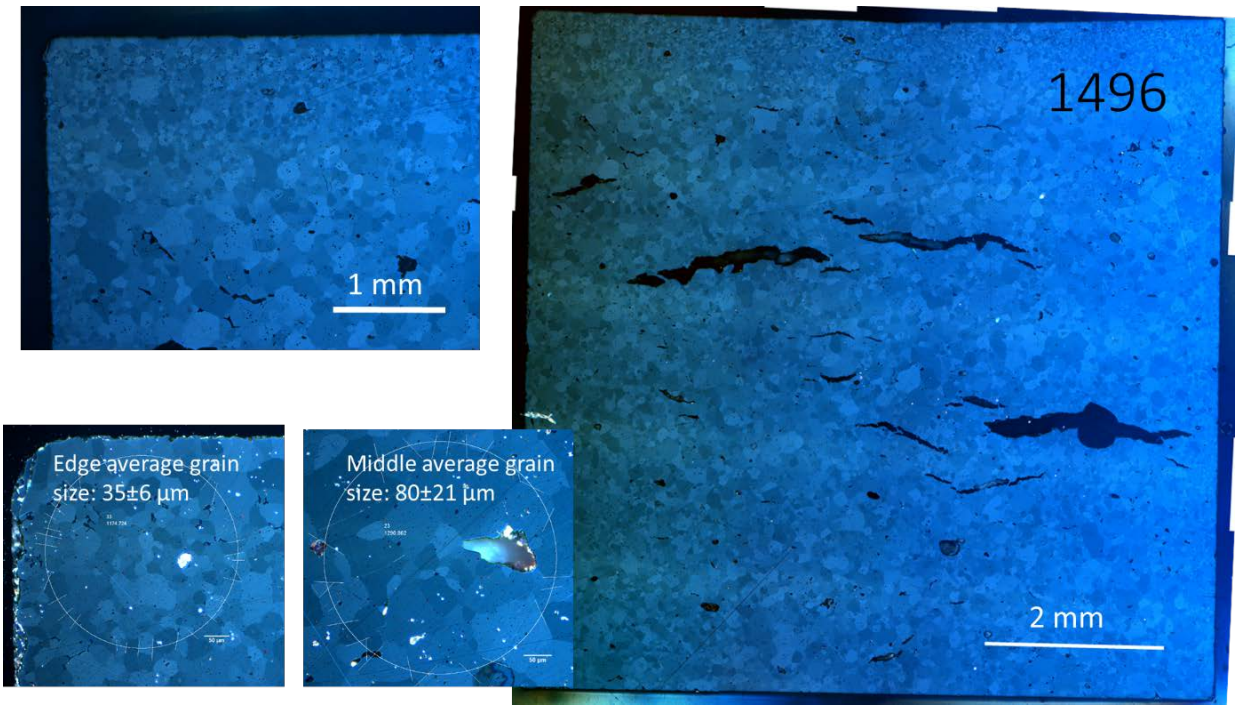

Figure 17. Longitudinal cross section of Sample 1496: example of bimodal grain growth with a coarse inner structure and fine non-continuous/uniform outer structure.

The grain structure of Sample 1459, Figure 18, was unique from other samples, showing three distinct grain size distributions: a fine outer structure, similar in size to what was observed in typical samples; then the largest grains measured, around 700 µm; and course inner grains, around 60 µm.

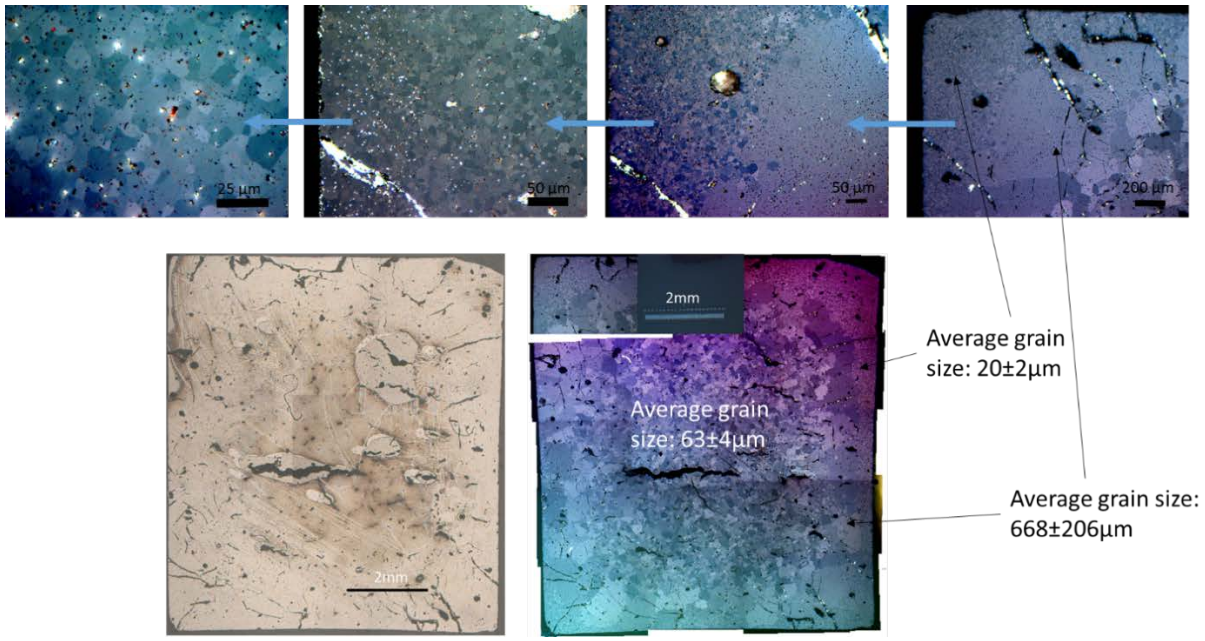

Figure 18. Sample 1459 optical images showing irregular mixed grain growth with fine grains around the edge, very large grains just within that and large grains in the center.

The grain size distribution measured for Sample ID 1476 was between 20 µm and 40 µm, with finer grains along the edge of the pellets and coarser grains inside, shown in Figure 19. The axial height of the radial cross section was not recorded. The smaller grain size observed in this batch may be related to the examination plane axial location near the surface of the pellet. However, a piece of a longitudinal cross section was also examined and displayed the same grain structure.

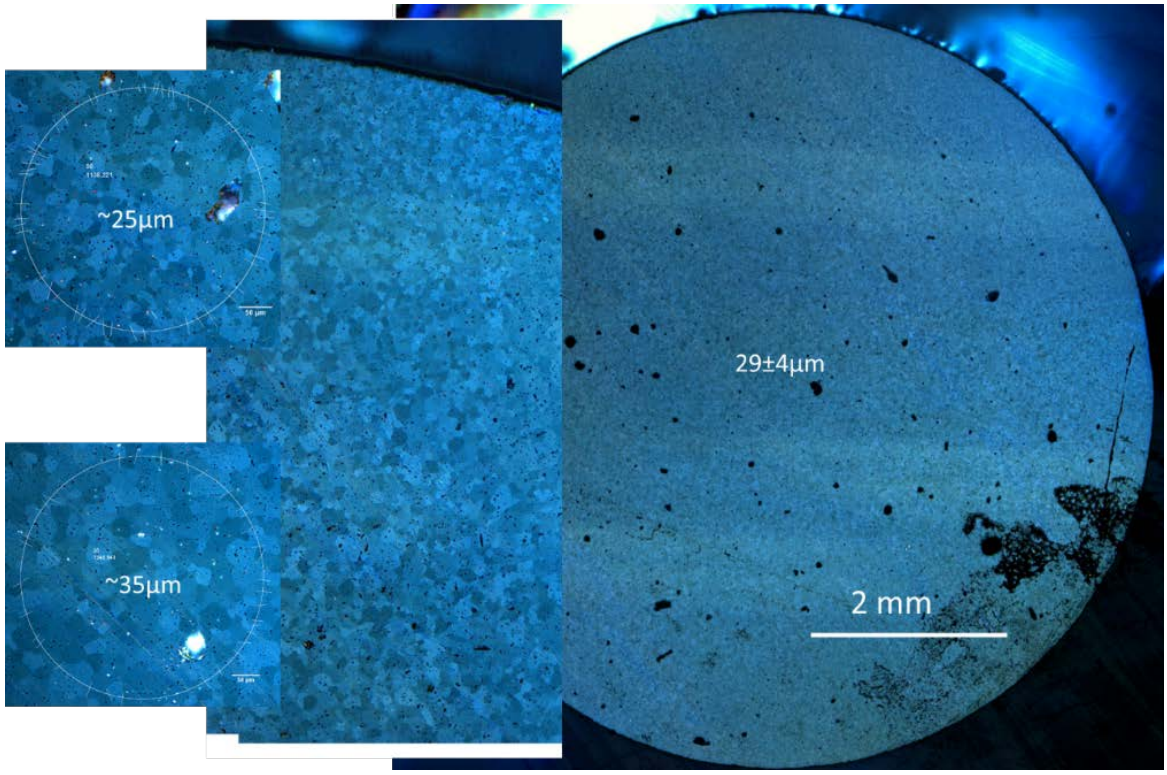

Figure 19. Radial cross section of Sample 1476 with enlarged regions to illustrate the slight gradient in grain size distribution from edge to center.

3.2 Phase Purity

Phase purity was measured on select representative ATF-1 pellets using an image analysis method in combination with EDS and XRD to verify phases. These measurements represent a baseline phase purity from the first round of U_3Si_2 pellet fabrication at INL. Ten pellet samples from extended fabrication efforts were also measured by the same methods, summarized in Table 4 and illustrated in Figure 20. Appendix B includes sample specific fabrication, measurement methods, raw data from image analysis, and subsequent phase quantification calculations. The Batch ID used throughout this section is roughly chronological and represents several years of process development. The measurements illustrate the increase in U_3Si_2 content as the pellet fabrication process matured, with a phase purity of up to ~98 vol. % U_3Si_2 achieved, improved from ~81 vol. % measured in the ATF-1 samples, and also reported by Harp et al. [2]

Table 4. Summary of phase measurements in ATF-1 and extended fabrication pellets.

Phase Purity of U_3Si_2 pellets for ATF-2 in vol. % via ASTM E1245 (SEM Image Analysis)					
Batch ID	voids	Fe phase	UO_2	Si rich phase	U_3Si_2
1005 (ATF1DU)	0.5±0.2	0.1±0.1	5.2±0.6	13.1±1.7	81.1±2.0
1108 (ATF1EU)	0.5±0.2	0.0±0.0	5.1±1.0	13.5±1.2	81.4±1.3
1270	0.6±0.3	0.2±0.0	3.7±0.8	8.0±0.3	87.5±1.1
1301	0.7±0.5	0.3±0.1	3.1±0.5	9.1±1.9	86.8±1.8
1336	1.4±0.7	0.4±0.3	2.9±0.9	3.6±0.5	91.7±2.3
1405	2.8±1.0		2.3±0.7	0	94.9±1.5
1425	1.2±0.8	0.2±0.1	1.9±0.5	0	96.9±1.3
1437	0.2±0.3	0.1±0.1	1.3±0.2	0	98.4±0.4
1459	0.7±0.5	0.2±0.1	1.7±0.5	0	97.4±0.7
1475	1.5±1.2	0.2±0.1	2.4±0.8	0	95.9±1.0
1476	0.6±0.3	0.2±0.0	2.9±0.4	0	96.2±0.6
1496	0.3±0.2	0.1±0.0	1.4±0.7	0	98.3±0.9

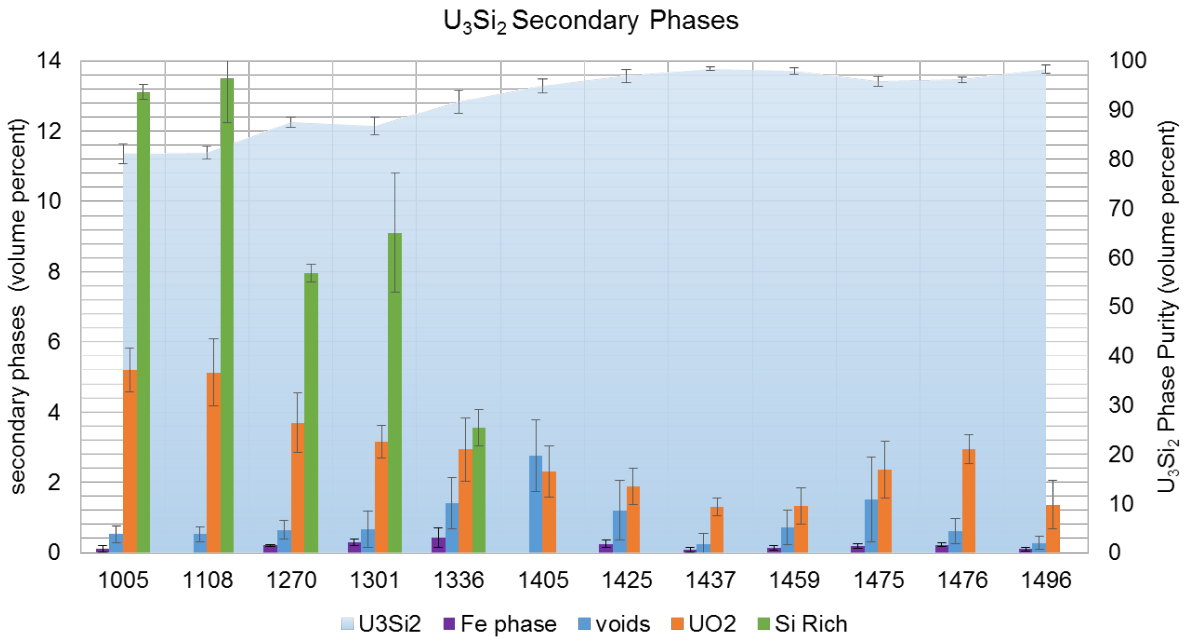

Figure 20. Representation of phase measurements as a function of volume percent in U_3Si_2 pellets.

It has been postulated [2,10] that the observed Si rich phases develop in U_3Si_2 as a result of UO_2 formation in the sample, leaving excess Si to form the U-Si phases that are higher in Si content than the matrix U_3Si_2 phase. An example of the Si rich phase is provided in Figure 8 where the Si rich phase has been colored in for threshold detection. ATF-1 samples have a mix of both USi and U_5Si_4 Figure 7. From the image analysis techniques described for discriminating between the two phases, the ATF-1DU sample had 1.5 ± 0.2 vol. % U_5Si_4 and 11.6 ± 1.5 vol. % USi. A silicon elemental map in Figure 7 illustrates the two different phases. The presence of two Si rich phases was also observed in XRD patterns for the same sample, shown in Figure 21. Crystallographic information for U_5Si_4 reported, by Noël et al., [10] and referenced previously for the characterization of similar samples, [9] was employed to identify this lighter contrast Si rich phase.

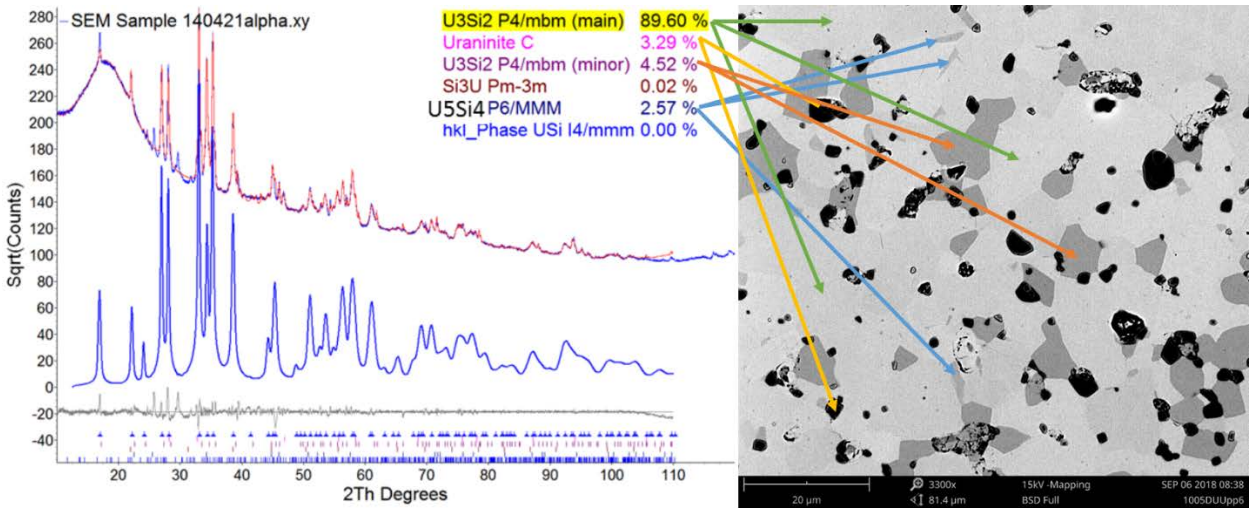

Figure 21. XRD spectra and BSE image of ATF-1 DU sample.

Automatic image analysis, performed on the same ATF-1 sample micrographs (example Figure 10), were in close agreement with the reported values (Table 4), measured via the manual method. Table 5 compares the values from the two methods and lists the percent difference in each value. The large % difference for the iron value is due to the small nature of the phase, which also was not as prevalent in the ATF-1 samples as it was in the extended fabrication samples. Each method had a large relative uncertainty for that phase. The percent difference in the UO_2 phase comes from a discrepancy in the two methods where the automatic method in some instances identifies an area as UO_2 while the manual method calls that same area a void. The areas of discrepancy likely occur where the sample has possible preparation-induced damage/pullout. The two methods are very close with the values for the Si rich phase and the U_3Si_2 phase.

Table 5. ATF-1DU sample phase quantification measurement comparison.

Comparison of manual vs. automatic image analysis phase quantification					
Method	**Phase/region**				
	voids	**Fe phase**	**UO_2**	**Si rich**	**U_3Si_2**
Manual	0.5±0.2	0.1±0.1	5.2±0.6	13.1±1.7	81.1±2.0
Automatic	0.4±0.3	0.3±0.3	7.0±0.9	13.1±1.1	79.2±1.6
difference	19%	-137%	-33%	0%	2%

According to XRD results for Sample 1301, Figure 22, the Si rich phase is likely U_5Si_4 and not the USi phase. The XRD results agree with SEM EDS data for both Samples 1301 and 1270. The only Si rich phase present in the extended fabrication pellets is likely U_5Si_4. In all samples fabricated with powder less than 80 days old, no excess Si phases were observed, with examples shown in Figures 24 and 25. Sample 1301 had a distorted "like - U_3Si_2" peak shift in XRD analysis shown in Figure 22 and compared with the XRD spectra of other samples with the same like- U_3Si_2 peaks in Figure 23. The like - U_3Si_2 peaks were observed in Samples 1405, 1425, and another DU extended characterization pellet batch (ID 1461) that was not fully characterized for this report. In Figure 23, the peaks of the main U_3Si_2 phase, with lattice parameters matching very closely to the published U_3Si_2 parameters, are marked with downward facing arrows. The like - U_3Si_2 phase peaks are marked with a smiley face. The UO_2 phase, present in all samples, is marked with a heart. As previously mentioned, the Sample 1301 also contains the U_5Si_4 phase, with peaks marked by a crescent moon.

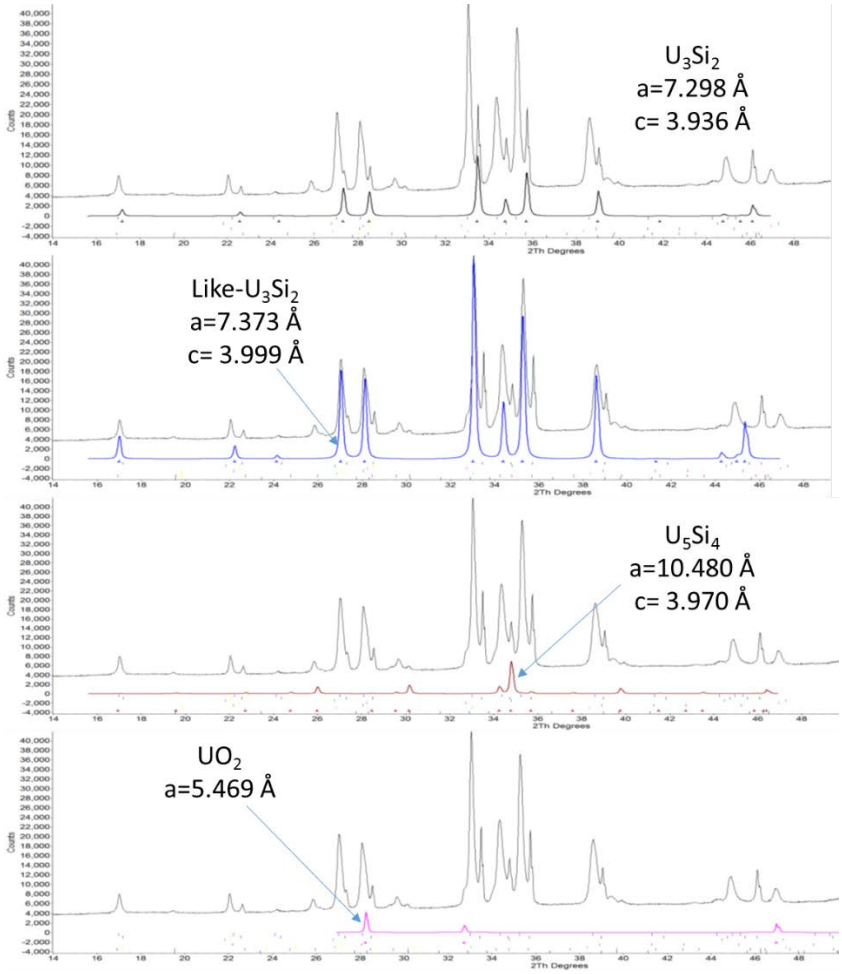

Figure 22. XRD spectra for Sample 1301 illustrating the main phase of U_3Si_2, the "like- U_3Si_2" phase, the U_5Si_4 phase, and the UO_2 phase.

XRD characterization on these samples (1301, 1405, 1425, and 1461) has proved inconclusive, as the semi-crystalline phase similar to U_3Si_2 (like - U_3Si_2), Figures 22 and 23, with strong diffracted intensities at dhkl = 2.713 Å and 2.547 Å, could not be matched by any published uranium silicide alloy.

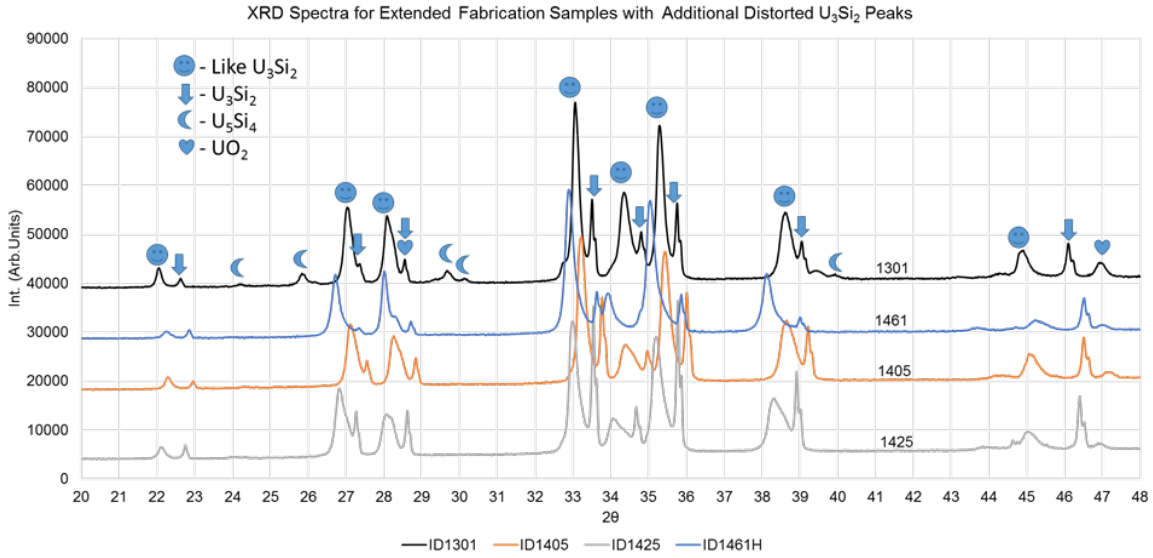

Figure 23. XRD spectra illustrating the main U_3Si_2 phase, the "like- U_3Si_2" phase, the UO_2 phase, and the U_5Si_4 phase.

Examples of pellets fabricated in the last half of the extended fabrication efforts are provided in Figures 24 and 25. Although these samples did have irregular grain growth, the phase distribution was homogenous across the sample and did not appear to be affected by the grain size inconsistencies.

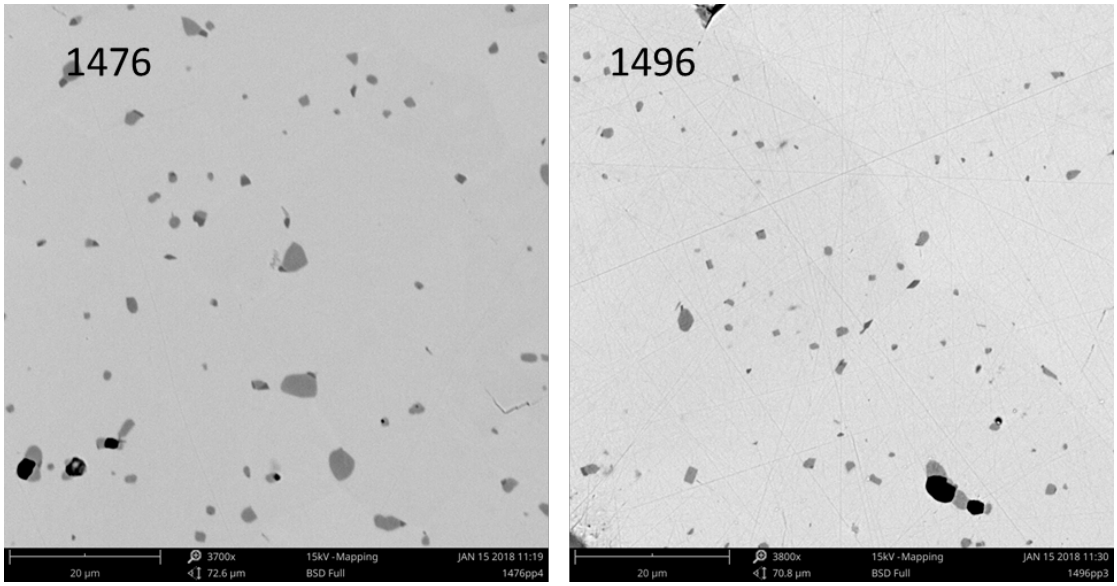

Figure 24. Extended fabrication U_3Si_2 pellet BSE micrograph examples.

In some samples, such as Sample 1459, extreme irregularities in grain growth were accompanied by cracking throughout the sample, illustrated by arrows in the BSE micrograph, Figure 25. The XRD spectra presented in Figure 25 for Sample 1459 is representative of the extended fabrication pellets made in the last half of fabrication efforts, including those shown in Figure 24, and all samples higher in number and including Sample 1437 (ID 1437, 1459, 1475, 1476). The preferred orientation/high intensity in the XRD peaks for these samples is attributed to the excessive grain growth forming a higher crystalline structure.

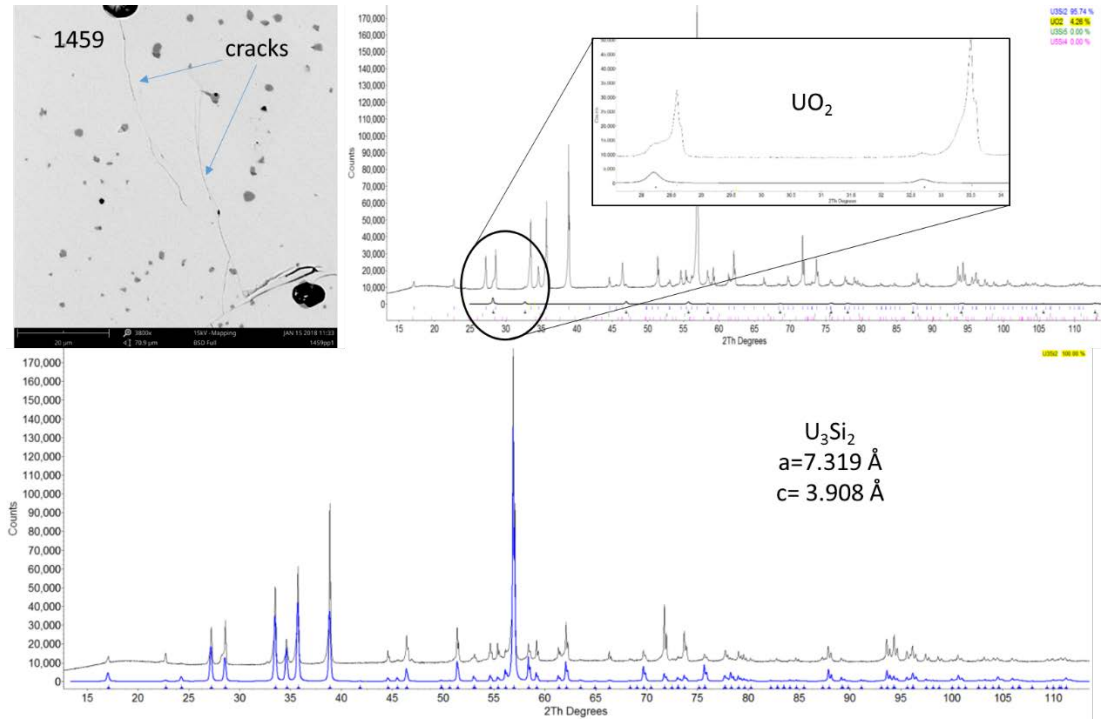

Figure 25. SEM BSE micrograph and XRD spectra for Sample 1459 with the blue line representing the calculated U_3Si_2 spectra and the black line representing the collected spectra, and an inset showing the location of the UO_2 peaks in the collected spectra.

4. DISCUSSION

The process parameter that seemed to have the biggest effect in reducing secondary phases within the U_3Si_2 pellets was the storage time elapsed between fabrication of the fine (~8 µm particle size [2]) U_3Si_2 powder and its pressing/sintering into pellets. Although the atmosphere of the storage argon glovebox is nominally maintained around 2 ppm O_2, because of the large surface area of the U_3Si_2 powder and uranium's affinity for oxygen, it was observed that the quantity of UO_2 phase measured in U_3Si_2 sintered pellets was directly proportional to the amount of time the powder had been stored in the glovebox. The powder used to fabricate Sample 1270 and 1301 remained in the glovebox over 100 days; therefore, a higher amount of oxygen was incorporated into the sample in the form of UO_2, as illustrated in Figure 26.

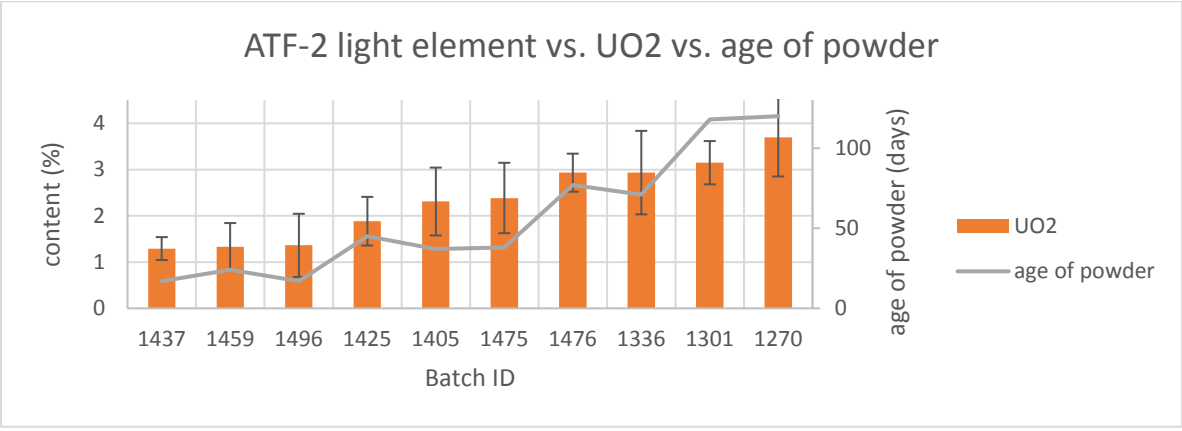

Figure 26. Correlation of volume percent UO_2 in U_3Si_2 pellets with age of U_3Si_2 powder.

The U_5Si_4 phase observed in both ATF-1 and some of the extended fabrication pellet samples is likely the result of powder oxidation while in the glovebox. The USi phase, observed only in ATF-1 samples, was a result of the original formulation (92.5 wt. % U, 7.5 wt. % Si) containing an excess of stoichiometric Si quantity. [2]

The origin of the like – U_3Si_2 phase observed during fabrication are not fully understood. They may stem from a variety of possible sources including hydrogen incorporation, carbon incorporation, or residual stress. The like - U_3Si_2 peak observed in early extended fabrication batches is very similar to the $U_3Si_2H_{1.8}$ peak reported by Mašková et al. caused by hydrogen atom insertion into the U_3Si_2 binary phase due to favorable uranium spacing within the U_3Si_2 unit cell. [12] The lattice parameters reported by Mašková for $U_3Si_2H_{1.8}$ are a=7.59Å and c=4.00Å. [12] The lattice parameters of the observed distorted like - U_3Si_2 peaks were on average a=7.42Å and c=3.98Å.

The U_3Si_2 fabrication process as outlined by Harp et al. [2] does introduce hydrogen initially to form fine U powder from U bar stock. This is done by a creating uranium hydride (thereby increasing the material volume) and subsequently dehydriding to form a porous material that is easily crushed into a fine powder. The process of flowing hydrogen over the uranium and vacuum pumping hydrogen off the uranium is done multiple times to reach the desired powder formation. [2] If the last step in this process is not adequately carried out, the resultant product may be uranium hydride powder. Inconsistencies in fabrication procedures during initial extended fabrication may have resulted in uranium powder that had not been fully dehydrided. All pellet samples composed of 100% hydride/dehydrided powder were observed to have this distorted U_3Si_2-like peak. Pellet samples composed of a mixture of the U_3Si_2 powder from an outside vendor and the hydride/dehydrided powder did not have this distorted like - U_3Si_2 peak in XRD, only the straightforward U_3Si_2 and UO_2 peaks.

Regardless of whether this initial uranium powder was fully dehydrided, the hydride should be removed in subsequent arc melting and sintering under dynamic vacuum at 1500°C for several hours. [2] This may also be confirmed by a measured hydrogen content (LECO OH 836 Analyzer) around 1 ppm for extended characterization samples. [13] However, prior to the hydrogen analysis, pellet samples were placed under dynamic vacuum for over 36 hours to remove any excess moisture they may have picked up during transfer to the test facility. [13] This vacuum drying may also be responsible for artificially dehydriding the pellets before measurement, but this is unlikely, as an elevated temperature is also required to remove hydrogen.

Mašková et al. did show that, upon cooling, rehydrogenation of U_3Si_2 at very low pressures can occur. [12] During U_3Si_2 pellet sintering, it is theoretically possible that hydrogen released during the sintering process was reabsorbed back into the pellets upon cooling, if the atmosphere of the furnace was not adequately removing excess gas. This is also unlikely as the vacuum was assumed to be in good working order for the duration of fabrication. The $U_3Si_2H_{1.8}$ phase requires hydrogen levels in excess of 2000 ppm. If the pellets did indeed include $U_3Si_2H_{1.8}$, their densities should reflect the higher volume phase with lower density values. Pellet densities, measured via He gas displacement pycnometry, for representative samples, were all very high, around 98% of the theoretical density of U_3Si_2.

Carbon insertion into U_3Si_2 has also been reported for several U-Si binary phases, including U_3Si_2 and U_5Si_4, producing the extended ternary phases $U_3Si_2C_{0.5}$ and $U_{20}Si_6C_3$, respectively. [10] Noel et al. reports that carbon insertion in U_3Si_2 results in an orthorhombic distortion of the lattice and an elongation of the lattice parameters, only slightly in the “a” direction, and from 3.89Å for U_3Si_2 to 10.41Å in the “c” direction. [10] This phase corresponds to 7700 ppm carbon.

Carbon enters the U_3Si_2 product at various stages in the fabrication process, as reported by Harp et al. [2] An organic lubricant during powder milling and binder during pellet formation, as well as sintering within a graphite furnace, may all contribute to elevated carbon levels within the samples. The temperature of sublimation for the organic additives is very low (below 600°C), and they are expected to

burn off during pellet sintering. The graphite furnace may also be a significant source of carbon in the pellets.

Samples from extended characterization were analyzed for carbon content (ELTRA CS800-Carbon/Sulfur) with values ranging between 1500 and 3500 ppm carbon, shown in Figure 24. The distorted XRD peaks observed in the first half extended fabrication samples are still in the P4/mbm space group with only slightly larger lattice parameters. It is not impossible that the distorted peaks are a result of this carbon atom insertion to a lesser extent that is not fully forming a ternary phase, but altering the lattice enough to show up as an extra U_3Si_2 peak. However, if carbon insertion were causing the like - U_3Si_2 peaks, those peaks should be present in all the samples with elevated carbon content. The samples with the highest levels of measured carbon were those fabricated in the later part of extended fabrication that had straightforward XRD spectra containing only U_3Si_2 and OU_2 peaks, as seen in Figure 27, no distorted like - U_3Si_2 peaks.

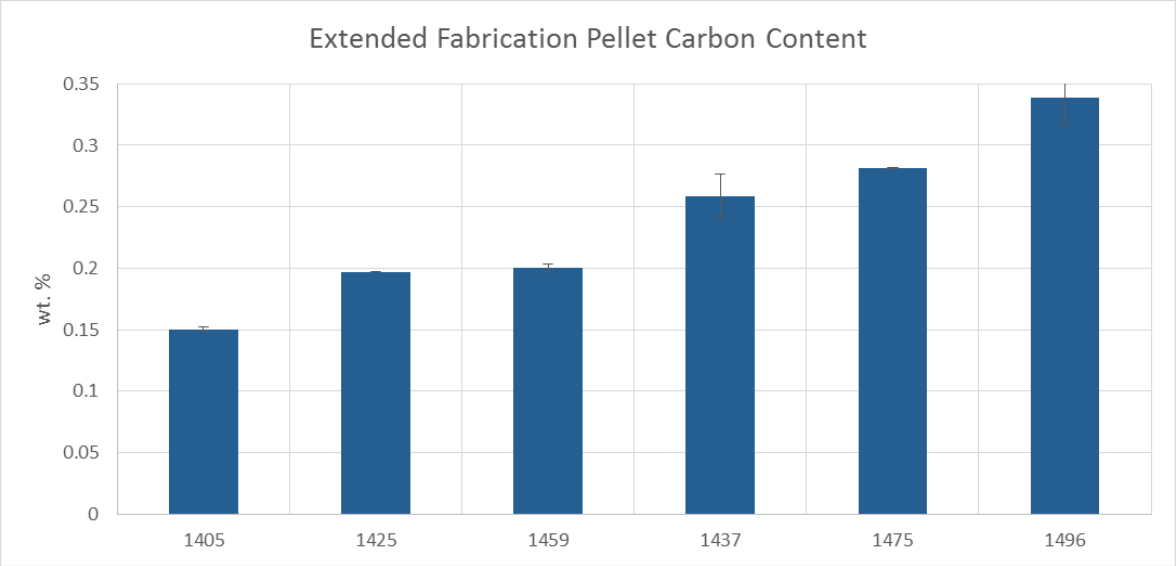

Figure 27. Carbon content of samples from extend fabrication sorted by carbon content: low to high.

Additional work is planned to re-examine some samples after an extended anneal has been done to determine if residual stress within the samples fabricated in the early half of extended fabrication may be causing the distorted like - U_3Si_2 phase.

5. CONCLUSIONS

The methods presented here provide a guideline for future characterization of U_3Si_2 pellet fuel. Processes to automate image thresholding and phase quantization increase efficiency and decrease operator bias of the measurements. A range of typical grain size, phases, and phase quantities have been identified for the U_3Si_2 pellet fuel system. A range of microstructural differences have been identified related to fabrication process changes or other sources of material contamination. Future perturbations from typical values presented here resulting from fabrication scale up and/or change in material feedstock would require additional investigation. Further investigation into the nature of irregular grain growth and possible unidentified (light element) contamination within specific U_3Si_2 samples is warranted.

The values presented here provide a baseline for microstructure characterization of as-sintered fresh fuel for comparison with irradiated samples as well as samples subjected to other various testing including diffusion couple interdiffusion investigations and thermal stability analysis. These methods and results will inform future fabrication efforts in order to further optimize pellet characteristics and provide a path for phase purity verification for quality control of future U_3Si_2 pellet fabrication efforts.

6. ACKNOWLEDGEMENTS

This work was supported by the US Department of Energy, Office of Nuclear Energy. This work is also part of a collaboration led by Westinghouse Electric Company, comprising several national laboratories, vendors, and universities awarded in response to the DE-FOA-00000712 funding opportunity. The authors would like to acknowledge the assistance of the support staff associated with the Fuels and Applied Science building at INL. Several technicians helped to contribute to this work including Seth Ashby, Kip Archibald, Wayne Poole, Andrea Wardle, Kevin Lamont, and Ginger Dexter. The authors would also like to acknowledge Tammy Trowbridge for her assistance with SEM image collection.

7. REFERENCES

1. INL/EXT-17-42155, GAIN Fuel Safety Research Workshop Summary Report, September 2017.
2. Harp et al., Uranium silicide pellet fabrication by powder metallurgy for accident tolerant fuel evaluation and irradiation, Journal of Nuclear Materials, 466 (2015) 728-738.
3. White et al., Thermophysical properties of U_3Si_2 to 1773 K, Journal of Nuclear Materials, 464 (2015) 275-280.
4. ASTM Standard E112-13, Standard Test Methods for Determining Average Grain Size, ASTM International, West Conshohocken, PA, 2003, www.astm.org.
5. ASTM E1245-03(2016), Standard Practice for Determining the Inclusion or Second-Phase Constituent Content of Metals by Automatic Image Analysis, ASTM International, West Conshohocken, PA, 2016, www.astm.org.
6. ASTM E1382-97(2015), Standard Test Methods for Determining Average Grain Size Using Semiautomatic and Automatic Image Analysis, ASTM International, West Conshohocken, PA, 2015, www.astm.org.
7. ASTM E883-11(2017), Standard Guide for Reflected–Light Photomicrography, ASTM International, West Conshohocken, PA, 2017, www.astm.org.
8. DeHoff, R. T., Quantitative Microscopy, Chapter 5, Measurement of number and average size in volume, pages 136–142. McGraw-Hill, 1st edition, 1968.
9. Hoggan, et al., Evaluation of U_3Si_2 fuel pellets sintered in an argon vs. vacuum environment, Presented at Material Science and Technology Annual Conference, October 2017.
10. Noel, H., S. Chatain, T. Alpettaz, C. Guéneau, C. Duguay, and J. Léchelle, Experimental Determination of (U-Si-C) Ternary Phase Diagram at 1000°C and Experimental Points in the Quaternary (U-Pu-Si-C) System, CNRS (2012).
11. Zuiderveld, Karel. “Contrast Limited Adaptive Histograph Equalization,” Graphic Gems IV. San Diego: Academic Press Professional, 1994, 474–485.
12. Mašková, S., K. Miliyanchuk, L. Havela, Hydrogen absorption in U_3Si_2 and its impact on electronic properties, J. Nucl. Mater., 487 (2017), pp. 418-423.
13. Xunxiang, Hu, Hydrogen and oxygen determination in as-fabricated U_3Si_2, Oak Ridge National Laboratory, ORNL/LTR-2018/8.

Appendix A

Grain Size Measurement Data Record

Appendix A

Grain Size Measurement Data Record

Batch ID	Specimen ID	Date of Test	U-Si amount	Sintering parameters		Additional Processing History	Method of Analysis	Plane examined	mean length	st. dv.	95%CI	%RA	# of Fields	95%CI multipliers	magnification	total length of test lines	total # of grains	specific location
	(Fab. date)			environment	heat schedule	age/source of powder			(μm)	(μm)						(μm)		
1005	130506βX4	5/23/17	92.5/7.5	argon	1500C4hr	ATF-1 early sample	circular	radial	45	4.4	6.13	13.70	4	2.776	200	4205.2136	94	—
1169	1a	2/17/18	92.7/7.3	vacuum	—	delayed	circular	radial	26	2.4	2.23	8.55	7	2.447	200	—	—	—
1169	2b	2/17/18	92.7/7.3	vacuum	—	delayed	circular	radial	28	3.6	3.73	13.27	6	2.571	200	—	—	—
1169	3c	2/17/18	92.7/7.3	vacuum	—	delayed	circular	radial	25	1.1	1.21	4.79	6	2.571	200	—	—	—
1005	140515γ	2/19/18	92.5/7.5	argon	1500C4hr	ATF-1 DU representative	circular	3 radial 3 longitudinal	18	3.3	3.45	19.43	6	2.571	200	4195.526	236	—
1005	130506γ4	5/23/17	92.5/7.5	argon	1500C4hr	ATF-1 early sample	circular	radial	38	4.1	5.11	13.48	5	2.776	200	5725.5388	151	—
1108	140409k	2/19/18	92.5/7.5	argon	1500C4hr	ATF-1 LEU representative	circular	radial	16	1.3	1.74	10.82	4	2.776	200	3011.372	187	—
1419	—	5/23/17	92.7/7.3	vacuum	—	quick (~14 days)	circular	radial	28	3.9	4.80	16.83	5	2.776	200	6181	217	—
1270	SEM sample	4/4/17	92.7/7.3	vacuum	—	120 days/ZPPR plate	circular	radial	29	3.5	4.38	15.22	5	2.776	200	5866.9644	204	—
1301	BSU NSUF	4/4/17	92.7/7.3	vacuum	—	118 days/ZPPR plate	circular	radial	31	1.8	2.54	8.16	4	2.776	200	4791.479	154	—
1301	SEM sample	4/4/17	92.7/7.3	vacuum	—	118 days/ZPPR plate	circular	radial	22	1.3	1.64	7.47	5	2.776	200	6451.8836	294	—
1336	—	3/1/18	92.7/7.3	vacuum	1500C5hr	71 days/ZPPR Plate	circular	radial	25	3.8	3.17	12.80	8	2.365	200	8410.399	340	—

Batch ID	Specimen ID	Date of Test	U-Si amount	Sintering parameters		Additional Processing History	Method of Analysis	Plane examined	mean length	st. dv.	95%CI	%RA	# of Fields	95%CI multipliers	magnification	total length of test lines	total # of grains	specific location
	(Fab. date)			environment	heat schedule	age/source of powder			(μm)	(μm)						(μm)		
1405	—	9/30/17	92.7/7.3	vacuum	1500C5hr	37 days/ ZPPR plate	circular	radial	25	3.7	4.59	18.23	5	2.776	200	16918.892	672	—
1425	—	9/20/17	92.7/7.3	vacuum	1500C5hr	51 days/ZPPR plate	circular	radial	29	1.9	2.30	7.84	5	2.776	200	11004.893	375	—
1437	—	9/21/17	92.7/7.3	vacuum	1500C5hr	17 days/BWXT	circular	longitudinal	28	2.6	3.19	11.60	5	2.776	200	2616.823	95	edge
1437	—	9/21/17	92.7/7.3	vacuum	1500C5hr	17 days/BWXT	circular	longitudinal	106	11.1	13.75	12.95	5	2.776	50	20806.308	196	middle
1459	—	9/21/17	92.7/7.3	vacuum	1500C5hr	24 days/BWXT	circular*	longitudinal	20	1.9	1.77	8.84	7	2.447	200,*500	3691.081	184	edge
									668	206.2	286.26	42.86	4	2.776	50	*measured individual grains		between
									63	3.6	4.45	7.09	5	2.776	50	12226.883	195	middle
1476	—	3/1/18	92.7/7.3	vacuum	1500C5hr	77 days/BWXT	circular	radial	29	4.4	3.12	10.64	10	2.262	200	12323.885	421	—
1496	—	3/13/18	92.7/7.3	vacuum	1500C5hr	17 days/BWXT	circular	longitudinal	36	5.8	6.07	17.06	6	2.571	200	6220.395	175	edge
1496	—	3/13/18	92.7/7.3	vacuum	1500C5hr	17 days/BWXT	circular	longitudinal	80	20.7	28.77	35.98	4	2.776	200	5516.88	69	middle

Appendix B

Phase Quantification Data Record

Appendix B

Phase Quantification Data Record

Batch ID	Sample ID	Enrichment % U-235	Feed-stock source	Age of Powder (days)	Magnification	# of fields measured	Measurement Area $(mm)^2$	Voids	Fe phase	UO_2	USi	U_5Si_4	Si Rich phases	U_3Si_2	
1005	140415	DU	N/A	unknown	3300	field 1	7	0.91	0.12	6.14	13.72	1.80	15.52	77.31	—
1005	140415	DU	N/A	unknown	3300	field 2	7	0.50	0.00	5.29	9.48	1.31	10.79	83.42	—
1005	140415	DU	N/A	unknown	3400	field 3	7	0.40	0.00	5.37	11.98	1.58	13.56	80.67	—
1005	140415	DU	N/A	unknown	3500	field 4	6	0.60	0.29	5.55	10.27	1.26	11.53	82.04	—
1005	140415	DU	N/A	unknown	3600	field 5	6	0.19	0.12	4.24	10.99	1.47	12.46	82.99	—
1005	140415	DU	N/A	unknown	—	total: 5	31	0.52	0.11	5.21	1.54	11.58	13.11	81.05	average
stdv	—	—	—	—	—	—	—	0.24	0.10	0.63	0.21	1.49	1.69	2.03	—
95%CI	—	—	—	—	—	—	—	0.30	0.12	0.78	0.26	1.85	2.10	2.52	—
%RA	—	—	—	—	—	—	—	57.05	112.69	14.91	17.11	15.96	16.04	3.11	—
1108	—	5%	N/A	unknown	—	—	—	—	—	—	—	—	—	—	—
1270	—	5%	HEU zipper plate	120	1000	field 1	3	2.11	0.06	4.19	—	8.47	—	85.17	—
1270	—	5%	HEU zipper plate	120	2000	field 2	3	0.37	0.20	4.79	—	8.25	—	86.40	—
1270	—	5%	HEU zipper plate	120	2000	field 3	3	0.77	0.22	3.05	—	7.59	—	88.36	—
1270	—	5%	HEU zipper plate	120	2000	field 4	3	1.04	0.15	4.24	—	8.14	—	86.43	—
1270	—	5%	HEU zipper plate	120	2000	field 5	3	0.42	0.24	2.71	—	7.85	—	88.78	—

Batch ID	Sample ID	Enrichment % U-235	Feed-stock source	Age of Powder (days)	Magnification	# of fields measured	Measurement Area $(mm)^2$	Voids	Fe phase	UO_2	USi	U_5Si_4	Si Rich phases	U_3Si_2	
1270	—	5%	HEU zipper plate	120	—	total: 4*	14	0.65	0.20	3.70	—	7.96	—	87.49	average
stdv	—	—	—	—	—	*lower mag. not counted	—	0.27	0.03	0.85	—	0.26	—	1.09	—
95%CI	—	—	—	—	—		—	0.34	0.04	1.05	—	0.32	—	1.35	—
%RA	—	—	—	—	—			52.23	19.72	28.46	—	3.98	—	1.54	—
1301	—	5%	HEU zipper plate	118	1000	field 1	3	1.12	0.33	3.50	—	9.05	—	86.00	—
1301	—	5%	HEU zipper plate	118	2000	field 2	3	0.18	0.20	3.66	—	10.99	—	84.99	—
1301	—	5%	HEU zipper plate	118	2000	field 3	3	0.21	0.44	3.45	—	8.62	—	87.28	—
1301	—	5%	HEU zipper plate	118	2000	field 4	3	1.45	0.33	2.43	—	6.22	—	89.57	—
1301	—	5%	HEU zipper plate	118	2000	field 5	3	0.83	0.23	3.06	—	10.61	—	85.28	—
1301	—	5%	HEU zipper plate	118	—	total: 4*	14	0.67	0.30	3.15	—	9.11	—	86.78	average
stdv	—	—	—	—	—	*lower mag. not counted	—	0.52	0.09	0.47	—	1.89	—	1.84	—
95%CI	—	—	—	—	—	—	—	0.65	0.12	0.58	—	2.35	—	2.28	—
%RA	—	—	—	—	—	—	—	97.03	39.18	18.46	—	25.82	—	2.63	—

Batch ID	Sample ID	Enrichment % U-235	Feed-stock source	Age of Powder (days)	Magnification	# of fields measured	Measurement Area $(mm)^2$	Voids	Fe phase	UO_2	USi	U_5Si_4	Si Rich phases	U_3Si_2	
1336	—	5%	HEU zipper plate	71	3300	field 1	7	0.621	—	—	—	—	—	—	—
1336	—	5%	HEU zipper plate	71	3800	field 2	5	1.39	—	—	—	—	—	—	—
1336	—	5%	HEU zipper plate	71	3800	field 3	5	1.053	—	—	—	—	——	—	—
1336	—	5%	HEU zipper plate	71	3800	field 4	5	2.778	—	—	—	—	—	—	—
1336	—	5%	HEU zipper plate	71	3800	field 5	5	1.215	—	—	—	—	—	—	—
1336	—	5%	HEU zipper plate	71	—	total: 5	26	1.4114	—	—	—	—	—	—	—
stdv	—	—	—	—	—	—	—	—	—	—	—	—	—	—	—
95%CI	—	—	—	—	—	—	—	—	—	—	—	—	—	—	—
%RA	—	—	—	—	—	—	—	—	—	—	—	—	—	—	—
1405	—	5%	HEU zipper plate	37	3000	field 1	8	1.42	—	1.57	—	—	—	94.98	—
1405	—	5%	HEU zipper plate	37	3000	field 2	8	4.04	—	1.61	—	—	—	92.66	—
1405	—	5%	HEU zipper plate	37	3000	field 3	8	1.90	—	2.16	—	—	—	94.25	—
1405	—	5%	HEU zipper plate	37	3000	field 4	8	1.61	—	1.90	—	—	—	95.80	—

Batch ID	Sample ID	Enrichment % U-235	Feed-stock source	Age of Powder (days)	Magnification	# of fields measured	Measurement Area $(mm)^2$	Voids	Fe phase	UO_2	USi	U_5Si_4	Si Rich phases	U_3Si_2	
1405	—	5%	HEU zipper plate	37	3000	field 5	8	3.48	—	3.56	—	—	—	92.27	—
1405	—	5%	HEU zipper plate	37	—	total: 5	40	2.76	—	2.31	—	—	—	93.74	average
stdv	—	—	—	—	—	—	—	1.03	—	0.73	—	—	—	1.35	—
95%CI	—	—	—	—	—	—	—	1.28	—	0.91	—	—	—	1.67	—
%RA	—	—	—	—	—	—	—	46.23	—	39.41	—	—	—	1.78	—
1425	—	5%	HEU zipper plate	51	3300	field 1	7	0.73	0.24	1.28	—	—	—	97.17	—
1425	—	5%	HEU zipper plate	51	3300	field 2	7	0.52	0.14	2.07	—	—	—	96.92	—
1425	—	5%	HEU zipper plate	51	3300	field 3	7	0.73	0.16	1.25	—	—	—	98.02	—
1425	—	5%	HEU zipper plate	51	3300	field 4	7	2.84	0.43	2.55	—	—	—	93.77	—
1425	—	5%	HEU zipper plate	51	3300	field 5	7	1.17	0.27	2.27	—	—	—	95.84	—
1425	—	5%	HEU zipper plate	51	—	total: 5	33	1.20	0.25	1.88	—	—	—	96.34	average
stdv	—	—	—	—	—	—	—	0.85	0.10	0.53	—	—	—	1.46	—
95%CI	—	—	—	—	—	—	—	1.05	0.13	0.65	—	—	—	1.82	—
%RA	—	———	—	—	—	—	—	88.05	51.21	34.64	—	—	—	1.89	—
1437	—	5%	BWXT powder	17	—	field 1	6	0.36	0.06	1.17	—	—	—	98.41	—

Batch ID	Sample ID	Enrichment % U-235	Feed-stock source	Age of Powder (days)	Magnification	# of fields measured	Measurement Area $(mm)^2$	Voids	Fe phase	UO_2	USi	U_5Si_4	Si Rich phases	U_3Si_2	
1437	—	5%	BWXT powder	17	—	field 2	6	0.78	0.20	1.29	—	—	—	97.73	—
1437	—	5%	BWXT powder	17	—	field 3	6	0.01	0.06	1.75	—	—	—	98.18	—
1437	—	5%	BWXT powder	17	—	field 4	6	0.01	0.07	1.24	—	—	—	98.68	—
1437	—	5%	BWXT powder	17	—	field 5	6	0.00	0.01	1.01	—	—	—	98.98	—
1437	—	5%	BWXT powder	17	—	total: 5	28	0.23	0.08	1.29	—	—	—	98.40	average
stdv	—	—	—	—	—	—	—	0.31	0.07	0.25	—	—	—	0.43	—
95%CI	—	—	—	—	—	—	—	0.38	0.08	0.31	—	—	—	0.53	—
%RA	—	—	—	—	—		—	163.51	101.30	23.81	—	—	—	0.54	—
1459	—	5%	BWXT powder	24	3800	field 1	5	0.87	0.14	1.23	—	—	—	97.76	—
1459	—	5%	BWXT powder	24	3700	field 2	5	0.07	0.08	1.34	—	—	—	98.51	—
1459	—	5%	BWXT powder	24	3600	field 3	6	1.40	0.23	1.58	—	—	—	96.80	—
1459	—	5%	BWXT powder	24	3600	field 4	6	0.54	0.23	2.52	—	—	—	96.71	—
1459	—	5%	BWXT powder	24	—	total: 4	21	0.72	0.17	1.67	—	—	—	97.44	average
stdv	—	—	—	—	—	—	—	0.48	0.06	0.51	—		—	0.74	—
95%CI	—	—	—	—	—	—	—	0.60	0.08	0.63	—	—	—	0.92	—
%RA	—	—	—	—	—	—	—	83.19	46.80	38.00	—	—	—	0.94	—
1475	—	5%	BWXT powder	38	2950	field 1	8	1.18	0.21	3.57	—	—	—	95.04	—
1475	—	5%	BWXT powder	38	2950	field 2	8	0.58	0.13	2.79	—	—		96.50	—

Batch ID	Sample ID	Enrichment % U-235	Feed-stock source	Age of Powder (days)	Magnification	# of fields measured	Measurement Area $(mm)^2$	Voids	Fe phase	UO_2	USi	U_5Si_4	Si Rich phases	U_3Si_2	
1475	—	5%	BWXT powder	38	2950	field 3	8	0.34	0.17	3.42	—	—	—	96.07	—
1475	—	5%	BWXT powder	38	2950	field 4	8	3.80	0.24	1.52	—	—	—	94.44	—
1475	—	5%	BWXT powder	38	2950	field 5	8	2.29	0.14	1.81	—	—	—	95.76	—
1475	—	5%	BWXT powder	38	2950	field 6	8	0.28	0.13	1.62	—	—	—	97.97	—
1475	—	5%	BWXT powder	38	2950	field 7	8	2.13	0.33	1.82	—	—	—	95.72	—
1475	—	5%	BWXT powder	38	—	total: 7	59	1.75	0.17	2.39	—	—	—	95.69	average
stdv	—	—	—	—	—	—	—	1.40	0.05	0.76	—	—	—	0.77	—
95%CI	—	—	—	—	—	—	—	1.74	0.06	0.95	—	—	—	0.96	—
%RA	—	—	—	—	—	—	—	99.35	32.95	39.61	—	—	—	1.00	—
1476	—	3.30%	BWXT powder	77	3900	field 1	5	0.65	0.22	2.82	—	—	—	96.30	—
1476	—	3.30%	BWXT powder	77	3700	field 2	5	0.33	0.17	2.91	—	—	—	96.59	—
1476	—	3.30%	BWXT powder	77	3700	field 3	5	0.65	0.22	3.72	—	—	—	95.41	—
1476	—	3.30%	BWXT powder	77	3700	field 4	5	1.22	0.32	2.68	—	—	—	95.78	—
1476	—	3.30%	BWXT powder	77	3700	field 5	5	0.22	0.20	2.54	—	—	—	97.05	—
1476	—	3.30%	BWXT powder	77	3700	total: 5	26	0.61	0.23	2.93	—	—	—	96.23	average
stdv	—	—	—	—	—	—	—	0.35	0.05	0.41	—	—	—	0.58	—
95%CI	—	—	—	—	—	—	—	0.43	0.06	0.51	—	—	—	0.72	—
%RA	—	—	—	—	—	—	—	70.36	26.74	17.40	—	—	—	0.75	—

Batch ID	Sample ID	Enrichment % U-235	Feed-stock source	Age of Powder (days)	Magnification	# of fields measured	Measurement Area $(mm)^2$	Voids	Fe phase	UO_2	USi	U_5Si_4	Si Rich phases	U_3Si_2	
1496	—	5%	BWXT powder	17	3800	field 1	—	0.49	0.09	1.37	—	—	—	98.04	—
1496	—	5%	BWXT powder	17	3800	field 2	—	0.02	0.09	1.58	—	—	—	98.30	—
1496	—	5%	BWXT powder	17	3800	field 3	—	0.31	0.11	1.13	—	—	—	98.45	—
1496	—	5%	BWXT powder	17	—	total: 3	—	0.28	0.10	1.36	—	—	—	98.26	average
stdv	—	—	—	—	—	—	—	0.19	0.05	0.68	—	—	—	0.86	—
95%CI	—	—	—	—	—	—	—	0.24	0.06	0.85	—	—	—	1.07	—